**RESEARCH ARTICLE**

# Rainfall types over southern West Africa: Objective identification, climatology and synoptic environment

Marlon Maranan | Andreas H. Fink | Peter Knippertz

Institute of Meteorology and Climate Research, Karlsruhe Institute of Technology, Karlsruhe, Germany

**Correspondence**
Marlon Maranan, Institute of Meteorology and Climate Research, Karlsruhe Institute of Technology, 76128 Karlsruhe, Germany.
E-mail: marlon.maranan@kit.edu

Southern West Africa (SWA) is characterised by a wide range of rainfall types, the relative importance of which have never been quantified on a regional level. Here, we use 16 years of three-dimensional reflectivity data from the Tropical Rainfall Measuring Mission–Precipitation Radar (TRMM-PR) to objectively distinguish between seven different rainfall types in three subregions of SWA.

Highly organized Mesoscale Convective System (MCS) events are the dominating rain-bearing systems in SWA. They tend to occur in highly sheared environments as a result of mid-level northeasterlies ahead of a cyclonic vortex. Their contribution to annual rainfall decreases from 71% in the Soudanian to 56% in the coastal zone. MCSs in SWA also propagate slower than their Sahelian counterparts and occur predominantly at the start of the first coastal rainy season. However, in terms of numbers, about 90% of rainfall systems are weakly organized classes, particularly small-sized, highly reflective and moderately deep (40 dBZ at altitude <10 km) systems. Contrary to MCSs, less organized convection typically occurs during and after the passage of a cyclonic vortex within a regime of deep westerly anomalies, low wind shear and low to moderate CAPE (convective available potential energy), bearing some resemblance to what has been termed "monsoon" or "vortex rainfall". Combining TRMM-PR rainfall system identification with infrared-based cloud tracking reveals that organized convection over SWA typically lasts for more than >9 h, whereas less intense rainfall types tend to be short-lived, diurnal phenomena. This novel approach stresses the relevance of mid-level (wave) disturbances on the type and lifetime of convective systems and thereby their regionally, seasonally and diurnally varying contribution to rainfall amount. The present study suggests further investigations into the character of the disturbances as well as possible implications for operational forecasting and the understanding of rainfall variability in SWA.

**KEYWORDS**

mesoscale convective systems; rainfall climatology; TRMM; West African monsoon

## 1 | INTRODUCTION

Rainfall over West Africa is mainly related to the West African monsoon (WAM) system and is known to vary considerably from year to year and on decadal time-scales (e.g. Diatta and Fink, 2014). Due to the prevalence of smallholder farming and rain-fed agriculture in West Africa, delayed onsets of the monsoon rains, monsoon breaks, flash floods, larger-scale seasonal inundations and longer-term droughts have large socio-economic impacts. Against these high vulnerabilities, disaster risk and mitigation measures are, amongst others, limited by the forecast skill of global numerical weather prediction models that barely exceeds climatology (Vogel et al., 2018), and by CMIP5 rainfall projections for

the 21st century that did not improve over the low confidence found in CMIP3 models (Christensen *et al.*, 2013, ). This poor performance of weather and climate predictions/projections is partly related to the convective nature of precipitation, as the employed models are unable to resolve the convective rainfall systems due to their coarse resolutions. In the literature, much attention has been devoted to a particular class of convective rainfall systems called Mesoscale Convective Systems (MCSs). This is the generic term for organized convective complexes with a horizontal extent of the precipitating area of more than 100 km in at least one direction (cf. Glickman and Zenk, 2000). Among the MCS category affecting West Africa, various authors have discussed squall- or disturbance-lines (e.g. Hamilton *et al.*, 1945; Eldridge, 1957; Aspliden *et al.*, 1976; Fink and Reiner, 2003), organized convective systems (OCSs; Mathon *et al.*, 2002), and mesoscale convective complexes (Laing *et al.*, 1999; Mathon *et al.*, 2002). The large attention paid to the understanding of the dynamics and climatology of MCSs can be explained by the fact that they bring up to 90% of the annual rainfall in the West African Sahel, a region that has been struck by extreme drought conditions in the 1970s and 1990s (Nicholson, 2013). Even though previous studies have long indicated an increasing role of other types of less-organized rainfall at the expense of MCSs towards the populous Guinea Coast (e.g. Acheampong, 1982; Omotosho, 1985; Kamara, 1986; Fink *et al.*, 2006), their spatio-temporally varying climatological roles as well as the (thermo-)dynamic environments in which they occur have never been thoroughly investigated in this region. The objectives of the present study are therefore (a) to define rainfall types and their climatologies for southern West Africa (SWA) based on data from the Tropical Rainfall Measuring Mission–Precipitation Radar (TRMM-PR), (b) to relate them to typical synoptic environments, and (c) to link them to previously known, infrared (IR)-based rainfall classifications. These will, inter alia, aid a better interpretation of weather and climate forecasts/projections, since larger-scale synoptic environments can be better represented than the rainfall itself.

Early descriptions of rainfall-producing cloud systems over SWA were based on recordings from ground-based weather stations and eye observations (Hamilton *et al.*, 1945; Eldridge, 1957) followed by quantitative analyses of rain-gauge measurements (e.g. Nicholson, 1979; Acheampong, 1982; Omotosho, 1984; 1985; Kamara, 1986). From these studies, three different rainfall types emerged. The first are local convective rainstorms, described as short-lived (1–2 h), stationary weather systems due to strong land surface heating, whose contribution to annual rainfall decreases from the coast (up to 50%) to the Savannah region of SWA (26% in northern Nigeria) (Acheampong, 1982; Omotosho, 1985). The second rainfall type, so-called monsoon rains, misses a clear definition, but is mostly considered as longer-lasting, steady (Kamara, 1986) or intermittent rainfall (Acheampong, 1982) falling out of deep-layered, mostly

non-thundery nimbostratus, altostratus or altocumulus clouds (Buckle, 1996). Their contribution varies from 28% to 52% at the coast to a mere 3.9% in the drier Soudan region. From our present understanding, the third category corresponds to the above-mentioned MCSs, most likely of squall-line type. A southward decrease of their rainfall fraction over SWA was noticed. It is well above 50% in the Soudan zone (Eldridge, 1957; Omotosho, 1985) and drops to 21% and 16% at the Nigerian and Ghanaian coasts, respectively (Acheampong, 1982; Omotosho, 1985). These pioneering studies have established that different surface characteristics of rainfall systems exist in SWA, but understandably a three-dimensional thermodynamic perspective was lacking or limited in the pre-satellite era.

With the advent of geostationary satellites in the early 1980s, numerous studies using passive infrared (IR) satellite imagery have advanced our understanding of West African rainfall systems. Desbois *et al.* (1988), Duvel (1989; 1990) and Rowell and Milford (1993), amongst others, discussed the diurnal, intraseasonal and interannual variability of convective cold cloud areas and their modulation by regional and synoptic-scale environmental conditions. Generally, high frequencies of cold clouds were found close to elevated terrain and in conjunction with mid-level wave disturbances, such as African Easterly Waves (AEWs). More recent work by Mathon and Laurent (2001), Fiolleau *et al.* (2009), Bennartz and Schroeder (2012), and Lafore *et al.* (2017b) for West Africa and Roca *et al.* (2014) for the global Tropics have provided further insights into the life-cycle and properties of MCSs. On average, they reveal that MCSs in the Sahel are faster and longer-lived and explain a higher percentage of total cloud cover (up to 90%, Mathon and Laurent, 2001) than over the coastal region (see also the C1 to C4 categorization in Lafore *et al.*, 2017b). However, the deficiencies of passive IR imagery to estimate rainfall have been known for a long time and are related to the indirect relationship between cloud-top temperature and rainfall (e.g. cirrus contamination), which varies substantially between different rainfall systems and between climatological regimes (e.g. Thiao *et al.*, 1990; Levizzani *et al.*, 2001; Kidd and Levizzani, 2011).

Some authors combined extensive rain-gauge measurements with IR-based tracking of cold cloud elements to infer the contribution of specific rainfall classes to total rainfall. For the Sahelian region around Niamey, Niger, Mathon *et al.* (2002) attributed 90% of total rainfall during the 1990–1999 period to so-called OCSs, a longer-lived and faster-moving sub-class of MCSs, which likely represent squall lines (Fink *et al.*, 2006). Their occurrence frequency is also assumed to determine the interannual variability of rainfall. In a similar approach, Fink *et al.* (2006) investigated the rainfall characteristics for the Upper Ouémé Valley in central Benin, located some 400 km south of Niamey in the Soudanian zone, during the 2002 rainy season. They found that MCSs accounted for 82% of total rainfall whereas around 9% were related to vortex rainfall. The latter had surface characteristics reminiscent

of the aforementioned monsoon rains and, in stark contrast to OCSs, were embedded in a regime of low CAPE (convective available potential energy) and low vertical wind shear. Overall, the results suggest a southward decrease of the contribution of MCSs to total rainfall over SWA and an increase of more isolated convective showers and monsoon rains, as speculated in Fink *et al.* (2006). Yet their and other studies were not able to provide any quantitative proofs.

The emergence of microwave (MW) sensors on Low Earth Orbit satellites in 1987 has significantly improved the rainfall estimation from space (e.g. Negri *et al.*, 1994; Kidd, 2001). Fink and Reiner (2003), for instance, used passive MW data to study the link between AEWs and squall lines in the 1998/99 monsoon seasons. Further technical advances culminated in the launch of the Tropical Rainfall Measuring Mission (TRMM) satellite (Kummerow *et al.*, 1998; Levizzani *et al.*, 2001) in 1997 which operated for more than 17 years. Mohr (2004) compiled the first in-depth study of organized convective systems for West Africa with data from the TRMM Microwave Imager (TMI) and emphasized the role of orography and the characteristics of organized convection as key factors to the understanding of the diurnal cycle of rainfall in the region. The TRMM also enabled the deployment of a precipitation radar (TRMM-PR; Kawanishi *et al.* (2000)) on its satellite which allowed for an active three-dimensional monitoring and subsequent characterization of convective cloud elements (Awaka *et al.*, 1997; Iguchi *et al.*, 2000). Various level-2 (i.e. orbital) TRMM-PR products have been used to investigate the variable nature of convection in the tropical belt (e.g. Houze *et al.*, 2007; Houze *et al.*, 2015; Romatschke *et al.*, 2010; Romatschke and Houze, 2010; Liu, 2011; Zuluaga and Houze, 2013; 2015). For most regions, Houze *et al.* (2015) noted that a large fraction of rainfall can be explained by the presence of so-called deep convective cores (DCCs), wide convective cores (WCCs) and broad stratiform regions (BSRs), each displaying, on average, different stages in the life-cycle of a mature MCS. In conjunction with the European Centre for Medium-range Weather Forecasts (ECMWF) ERA-Interim reanalysis data, Zuluaga and Houze (2015) found that mesoscale convection (WCC, BSR) is linked with AEW disturbances in the Soudano-Sahelian region. They occur ahead of the wave trough and under the influence of convergent flow at low levels. The relationship between TRMM-PR rainfall events and their respective environment over West Africa was further investigated by Janiga and Thorncroft (2014) and Janiga and Thorncroft (2016). They concluded that CAPE, vertical wind shear and the column relative humidity are decisive factors that control the characteristics of convective systems. Their distribution over West Africa is, in turn, assumed to be latitude- and AEW phase-dependent. They suggest that the rainfall maximum shifts from the maximum northerlies for the Sahel to the more humid trough region for SWA.

In a novel and comprehensive approach, the present study exploits the advantages of TRMM-PR and the Meteosat IR imagery to create an extensive climatology of rainfall characteristics with a combined multi-satellite dataset for the understudied SWA region. The study is based upon, extends and regionalizes the rainfall system characterisation used in Houze *et al.* (2015). It will provide an assessment of the seasonal and diurnal cycles in frequency of occurrence as well as the contributions to total rainfall. The rainfall types identified will be related to known IR-based classifications of convective systems. Composite cross-sections of meteorological fields are used to determine their specific pre- and post-event environments.

Section 2 details the data sources and how they were processed. In section 3 the rainfall categories are presented as well as the cloud tracking routine used to investigate the life-cycle of the convective systems. Section 4 gives an overview of the rainfall distribution over SWA represented by TRMM-PR before the contribution of the rainfall classes is analysed in section 5. Section 6 investigates the environmental conditions for the rainfall types, while in section 7 the convective elements from TRMM-PR are connected with IR cloud tracking data. Finally, in section 8 a brief summary of the study and concluding remarks are given.

## 2 | DATA SOURCES AND PROCESSING

### 2.1 | TRMM Precipitation Radar products

The TRMM-PR orbited the earth at an altitude of 402.5 km (350 km before August 2001) scanning with a swath width of 247 km (215 km) with a surface horizontal resolution of 5 km (4.3 km) at the Earth's surface (Kummerow *et al.*, 1998; Kawanishi *et al.*, 2000). The resolution in the vertical is 250 m with the highest layer at 19.75 km. Convective systems are investigated using the level-2 products 2A25 and 2A23 (V7) from the TRMM-PR (Iguchi *et al.*, 2000) for the period from 1998 to 2013. Data from 2014 were discarded due to shut-down preparations during the same year (Houze *et al.*, 2015). The 2A25 dataset contains the three-dimensional, attenuation-corrected radar reflectivities and rain-rate profiles (Heymsfield *et al.*, 2000), while the 2A23 dataset provides information about the rainfall type (convective, stratiform, other). These two products were used for the classification of rainfall systems (section 3). The radar swath intersected the wider study area displayed in Figure 1 on four to six occasions per day at no specific location and time of day. Thus, the TRMM-PR dataset does not provide continuous observations in space and time, but provides random instantaneous values from different stages in the life-cycles of convective systems. The instantaneous rainfall rates in the 2A25 product are given in mm h$^{-1}$ and in the present study all statistics are inferred as if the "lifetime" of all rainfall elements is 1 h.

For a more convenient comparison with the other datasets described in this section, the data were re-gridded from their native non-Cartesian geolocation onto a 0.05° × 0.05° spaced
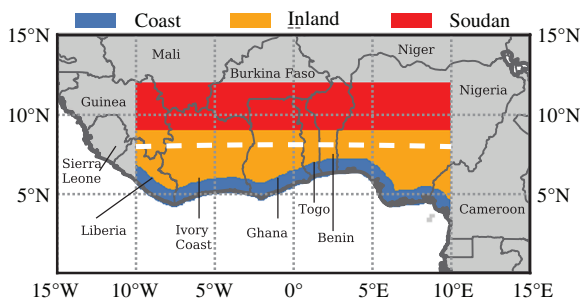
**FIGURE 1** Definition of the subregions used in section 5: the "Coast" in blue which encompasses all pixels within a 100 km distance from the coastline, the "Inland region" as far north as 9°N in orange and the "Soudanian region" in red from 9 to 12°N. All regions are zonally bounded between 10°W and 10°E. The dashed white line at 8°N denotes the latitude which was taken to construct the time–height cross-sections shown Figure 7 [Colour figure can be viewed at wileyonlinelibrary.com]

latitude–longitude grid based on the procedure described in Houze *et al.* (2007). Furthermore, while retaining the vertical resolution, a correction of the vertical geolocation was performed. Since the same coordinates are stored at all height bins along the radar beam, a horizontal offset is introduced which gets larger with greater elevation. By removing this offset, a correction of radar echo structures is performed as well.

## 2.2 | Meteosat SEVIRI infrared imagery

Convective cloud features were tracked using the infrared dataset (Channel 9 at approximately 10.8 $\mu$m) of the Spinning Enhanced Visible and Infrared Imager (SEVIRI) on the Meteosat satellite operated by the European Organisation for the Exploitation of Meteorological Satellites (EUMETSAT). Before applying the actual tracking procedure (section 3), the native radiance datasets were first converted into brightness temperature fields by using the approach presented in Tjemkes (2005). The dataset comes on an irregular horizontal grid with a spacing of 3 km at the sub-satellite point on a 15 min basis, allowing for an assessment of the history of the convective systems before and after the TRMM overpasses. To ensure comparability, the fields were interpolated onto the same grid as the TRMM-PR data. However, since it is known that convective systems originating as far east as 30°E can influence West Africa (e.g. Laing *et al.*, 2008), the data and tracking were extended eastward to this longitude. While the TRMM-based rainfall classification was performed for the whole year between 1998 and 2013, IR-based system tracking was only performed during the major rainy seasons between April and October and only for the SEVIRI 2004–2013 period.

## 2.3 | Global reanalysis data

Three-dimensional, six-hourly ECMWF Interim reanalysis (ERA-Interim) fields (Dee *et al.*, 2011) on a 0.75° grid

are used to investigate the environmental conditions around rainfall events. All available pressure levels from 1000 to 100 hPa were considered. In a further step, long-term mean fields were created to enable an analysis of anomalies. Here, the reference period is 1998–2013 in accordance with the TRMM-PR period.

## 3 | METHODS

### 3.1 | TRMM-PR based classification of rainfall types

Rainfall systems in the TRMM-PR data are classified based on the method described in Houze *et al.* (2007; 2015), who applied structure-based thresholds on the three-dimensional radar echoes. Here we also consider two additional categories of convective systems (MOD and STR, see below). These were omitted by other authors because of their relatively low contribution to total rainfall in the entire Tropics and Subtropics (Houze *et al.*, 2015) but over SWA they turn out to be of some relevance.

As in Houze *et al.* (2015), rainfall elements are identified by filtering areas of at least two neighbouring pixels with a radar signal. As this study focuses on convective systems over land, a stricter threshold of 40 dBZ is applied (Houze *et al.*, 2007; Houze *et al.*, 2015; Romatschke and Houze, 2010). The existence and the structure of 40 dBZ cores within the contiguous, three-dimensional echo volumes of convection determines which category the rainfall system falls into. The following categories are considered for further analyses.

- Isolated shallow echo (ISE) is the only pure warm-rain category that is identified. Signals from this shallow convective type are included in the 2A23 product and indicate isolated systems with an echo top of at least 1 km below the climatological freezing level (4.5 km) (Schumacher and Houze, 2003).
- Moderate convection (MOD) is used for convective volumes whose cores do not exceed a reflectivity of 40 dBZ and that are not ISEs. MODs are introduced here as one of the two additional categories to extend the analysis to weaker convection.
- If an 40 dBZ core is found in the convective volume, it is classified as strong convection (STR) at first. This remains as long as the definitions of the subsequent categories are not fulfilled. STR is the second category that is added in this study.
- A deep convective core (DCC) is identified if a 40 dBZ core exceeds the altitude threshold of 10 km above mean sea level.
- Wide Convective Cores (WCCs) are rainfall systems where the horizontal extent of ground-projected 40 dBZ cores reach at least 1000 km². Zuluaga and Houze (2015) attribute systems with such extensive convective areas to larger convective complexes with a high degree of organization. It should be noted that a height criterion is

not applied here, meaning that DCCs and WCCs do not coincide.

- If the height criterion for DCCs and the area criterion for WCCs are fulfilled at the same time, we assign the system to a new category called deep and wide convective core (DWC). As such, DWCs are treated here as a discrete rainfall category and are therefore not subsets of either DCCs or WCCs.

- Convective elements with a horizontal stratiform echo of at least 50,000 km$^2$ are called broad stratiform regions (BSR). Here, the 40 dBZ criterion is not a necessary condition since such large, contiguous stratiform regions are most likely linked to mature MCSs (Houze, 2004) that emanated from the categories above.

Although all categories are disjunct, we emphasize the possibility that successive TRMM overpasses may sample the same convective system during different stages and thus it may be allocated to different categories. However, given that on average every radar pixel is sampled once about every 3 days (section 4), this only applies to few long-lived and/or fast moving systems.

## 3.2 | Tracking of convective clouds with SEVIRI data

A slightly modified version of the tracking routine introduced in Schröder *et al.* (2009) was applied which, in essence, is a combination of the methods of Williams and Houze (1987) and Mathon and Laurent (2001). Cloud pixels in the brightness temperature fields were first identified by applying a threshold of 233 K and then connected using an eight-pixel neighbour algorithm, resulting in contiguous cold cloud areas. This temperature threshold has been widely used in order to delineate cloud areas in tropical regions with potential rainfall (Arkin, 1979; Mathon and Laurent, 2001; Fink *et al.*, 2006).

As in Schröder *et al.* (2009), a minimum threshold of 900 km$^2$ for clouds ($\approx$ 36 pixels in the interpolated SEVIRI

data at nadir) is chosen to track smaller, non-MCS type, systems while maintaining robustness in tracking. The actual tracking method contains an area overlap approach. The assignment of clouds in two successive IR images at $t_0$ and $t_1$ is determined by a forward ($t_0 \rightarrow t_1$) and backward ($t_1 \rightarrow t_0$) similarity analysis of area overlap, horizontal translation of the centre of mass and the difference in cloud size as described in Schröder *et al.* (2009). However, an assignment between a cloud pair is only possible if an area overlap of at least 50% in either forward or backward analysis is reached. Visual inspection of tracks from slow- and faster-moving cases over SWA showed that the assignment of clouds with this overlap threshold and a size cut-off of 900 km$^2$ are overall plausible, as long as successive images on a 15 min basis are used. The definition of split and merger events are adopted from Mathon and Laurent (2001). Here, the most similar cloud at $t_1$ receives the same label as the parent cloud at $t_0$, whereas the other system undergoes a so called "split generation" or "merger end."

## 4 | RAINFALL CLIMATOLOGY FROM TRMM-PR

In this section, we first examine the spatial rainfall climatologies over SWA based on the instantaneous 2A25 rainfall rates to assess possible impacts of the sampling. For this purpose, the spatial distribution of the mean annual rain rate and the diurnal harmonic phase of rainfall over SWA based on the TRMM-PR 2A25 product are presented in Figure 2. Here, the mean rain rate at a pixel was first calculated as the average rain rate of all overpasses (originally in mm h$^{-1}$) and then served as a basis for an annual estimate. A given pixel over SWA was scanned over 2000 times by the TRMM-PR during the mission period, equivalent to one overpass every 3 days statistically. It can be seen that the pixel-to-pixel variability of rainfall rate based on TRMM-PR is quite high (Figure 2a). This has two primary reasons: (a) the randomness in overpasses
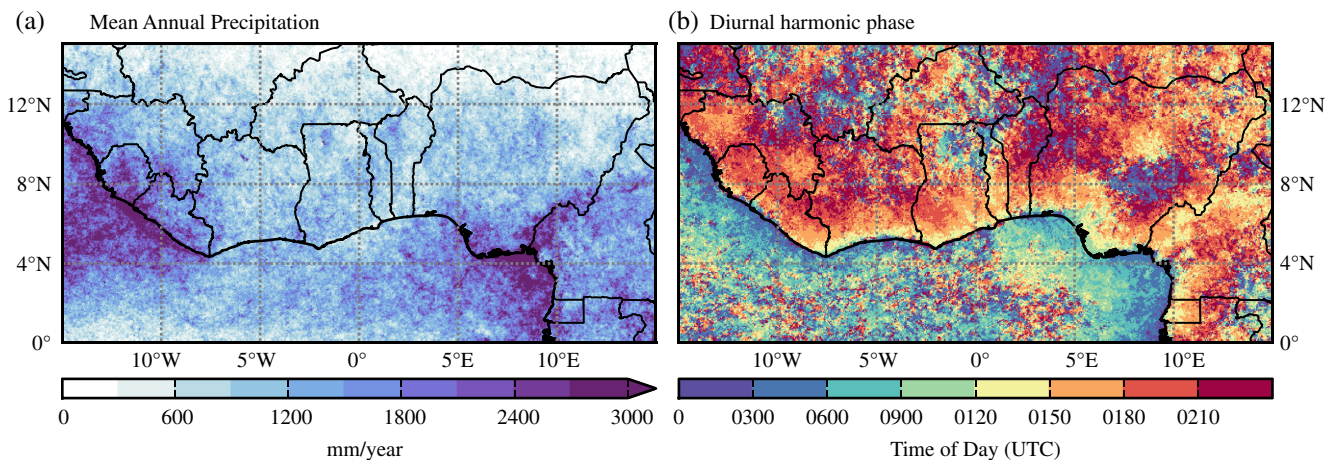


**FIGURE 2** TRMM-PR-based rainfall maps over SWA: (a) the mean annual precipitation and (b) the phase of the diurnal harmonic based on >2000 overpasses over a given pixel during the period 1998–2013. For (a), the accumulated rainfall rate in the TRMM 2A25 product was divided by the number of TRMM-PR overpasses for each pixel and then used for an annual estimate. The diurnal phase was computed through discrete Fourier transformation. UTC roughly corresponds to local time [Colour figure can be viewed at wileyonlinelibrary.com]

and time of day, and (b) a more detailed representation of smaller-scale, more intense convective parts of the rainfall systems by TRMM-PR, which can leave isolated footprints of higher rainfall amounts. However, the overall rainfall distribution in TRMM-PR over SWA exhibits spatial structures well-known from the literature, for instance the wet Adamawa Mountains and Niger Delta (e.g. Vollmert *et al.*, 2003) and the strong meridional gradient in rainfall amount towards the Sahel (e.g. Fink *et al.*, 2017).

Despite the highly variable pattern in the TRMM-PR rainfall field, the spatial distribution of its mean phase of the diurnal harmonic reveals some coherent signals (Figure 2b). The most striking feature is the difference in the diurnal peak of rainfall over land and sea. Over the ocean close to the coastline, convection is most active during the night and early morning. The mean phase shifts to after sunrise towards open waters, especially over the convectively active Bight of Bonny (3°N, 8°E) (also Negri *et al.*, 1994). Over land near the coast, the phase of most active rainfall is from noon to early afternoon. Apparently, the land/sea-breeze circulation is the driving force for rainfall here, but rainfall systems may also migrate northwards (Parker *et al.*, 2017). This is in accordance with findings in Yang and Slingo (2001), Derrien and Le Gléau (2005) and He *et al.* (2015), where a strong meridional phase shift in time of cold cloud and rainfall patterns at the coast is evident. The diurnal phase shifts gradually towards late afternoon and eventually early evening hours farther inland. Farther north at some distance from the coast, coherence becomes less pronounced, which reflects a higher spatial variability of the diurnal cycle. While this is suggested to be a consequence of a sampling issue to first order, variations in lifetime and translation speeds of MCSs as well as the gradual northward decrease of annual rainfall might further contribute to the higher spatial variability of the diurnal phase. Overall, the described patterns are similar to those presented in Janiga and Thorncroft (2014), who investigated

the period July–September during 1998–2012. This indicates that these three peak rainy season months alone contribute substantially to the diurnal variation over SWA.

For the upcoming analyses in section 5, the SWA domain from 10°W to 10°E was subdivided into three regions (Figure 1).

- The Coast region, representing the 100 km wide strip of land along the coastline;
- The Inland region, bounded to the south by the Coast region and extending northwards up to 9°N;
- The Soudanian region, the northernmost subregion of SWA from 9 to 12°N.

The decision to separate the coastal strip from the Inland region is related to the fact that the former is influenced by land/sea-breeze convection as suggested by the morning peak in rainfall (Figure 2b). The Soudanian zone is defined with reference to Fink *et al.* (2006; 2017) and is regarded as the transition region between the more humid Guinea coast region to the south and the drier Sahel to the north.

The annual cycle of TRMM-PR rainfall in each of the subregions is shown in Figure 3a. The profiles emphasise the progressive meridional change in seasonal rainfall. The Coast region exhibits a bimodal cycle with a clear primary rainy season peaking in June and a secondary maximum in September and October during the southward retreat of the rainbelt. This bimodal configuration is also seen for the Inland region where, however, the monthly accumulated rainfall during the southward retreat of the rainbelt in September is somewhat higher than earlier in the year. Over both the Coast and Inland regions, the monthly rainfall decreases from June to July and a local minimum is found in August, marking the so-called "little dry season" (e.g. Nicholson, 1981; Le Barbé *et al.*, 2002; Vollmert *et al.*, 2003). In contrast, the Soudanian region is characterized by an unimodal profile that peaks in August. This is generally consistent with annual profiles of
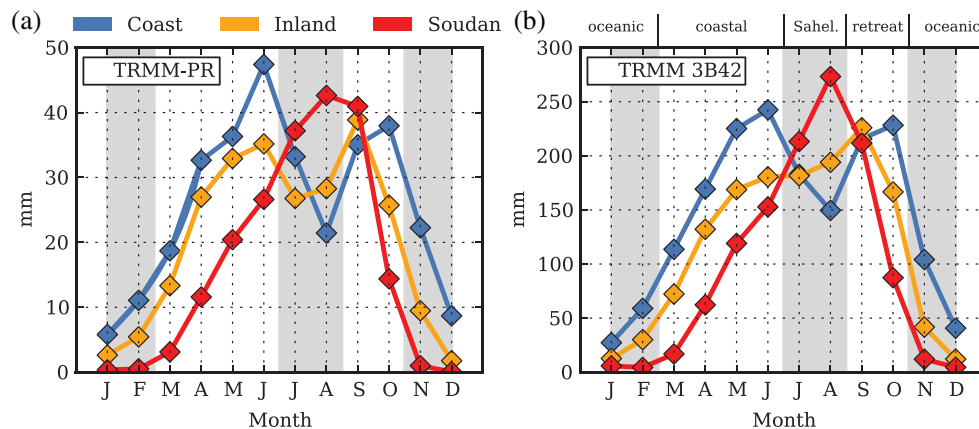


**FIGURE 3** Region-averaged annual profiles of accumulated rainfall for (a) TRMM-PR and (b) TRMM 3B42. The shadings denote different phases of the rainy season over SWA (after Thorncroft *et al.* (2011) with small amendments): the oceanic phase from November to February, the coastal phase from March to June, the Sahelian phase from July to August and the retreat phase from September to October (also indicated at the top of (b)). Note the different scales of the ordinate between (a) and (b). For TRMM 3B42, the entire continuous 3-hourly record from 1998 to 2013 was used to compile the profiles in (b) whereas (a) is based on >2000 overpasses over a given pixel [Colour figure can be viewed at wileyonlinelibrary.com]

(a)



(b)
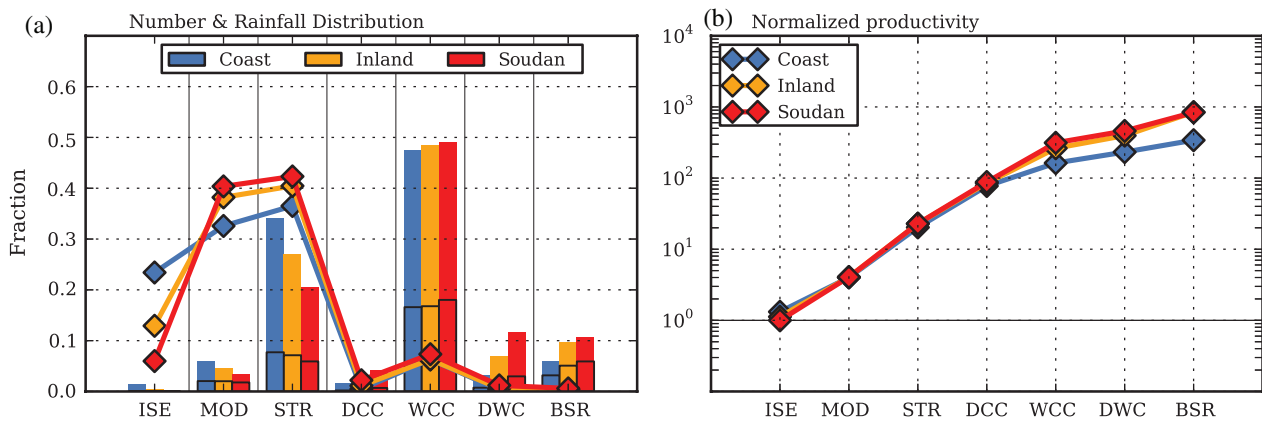
**FIGURE 4** Occurrence frequency, rainfall contribution, and rainfall productivity per type. (a) Fractional contribution of each rainfall category in each subregion to the number of events (lines) and rainfall amount (bars). The black framed bars indicate the fraction of stratiform rainfall. (b) Normalized rainfall amount of each rainfall category in each subregion relative to the mean rainfall amount of ISEs in the Soudanian region, which is the lowest of all values [Colour figure can be viewed at wileyonlinelibrary.com]

raingauge-based data (Judex and Thamm, 2008; Dezfuli et al., 2017; Fink et al., 2017) in the respective regions. Compared to the gridded, three-hourly TRMM product 3B42 (Figure 3b), the monthly rainfall totals are considerably lower. Again, this is the result of the discontinuous sampling of TRMM-PR in space and time. Nonetheless, the fundamental differences between the subregions with respect to the annual cycle are reasonably captured by TRMM-PR, with the exception that a clear bimodal configuration is absent for the Inland region in TRMM 3B42.

To provide a better orientation for the remainder of the manuscipt, we subdivide the different phases of the West African rainy season and, hereafter, label the months November to February as oceanic phase, March to June as coastal phase, July to August as Sahelian phase and September to October as retreat phase, indicated as alternating shading in Figure 3. This discrimination is a slightly amended version of the definitions made in Thorncroft et al. (2011), who relate the different phases to the position of maximum moisture flux convergence and thus the position of the rainfall belt. The beginning of the Sahelian phase is also termed "monsoon onset" by many authors (e.g. Sultan and Janicot, 2003; Parker et al., 2005a; Thorncroft et al., 2011; Fitzpatrick et al., 2015).

## 5 | SPATIO-TEMPORAL CLIMATOLOGIES OF RAINFALL TYPES

### 5.1 | Number and rainfall contribution

The contribution to the total number of events and the amount of rainfall of all categories defined in section 3 across the regions are presented in Figure 4a. As can be inferred from the diamond markers, 89% (Soudanian region) to 92% (Coast) of all identified convective elements are ISEs, MODs or STRs. The relative number of ISEs at the Coast is about 18% higher than in the Soudanian region. Being typical for the ocean (Schumacher and Houze, 2003; Houze et al., 2015), it indicates the more maritime environment of the coastal region

that is established through land/sea-breeze interactions. The occurrence frequency of deep and wide categories is fairly uniform across SWA, where WCCs account for around 7% of all systems. In contrast to its numbers, WCCs alone dominate the contribution to total rainfall and produce almost half in any region. Combined with contributions from DWCs and BSRs, this contribution increases to 56% at the Coast region and to 71% in the Soudanian region. As they represent the MCS-type elements, the latter fraction is comparable with findings in Fink et al. (2006), who attributed around 82% of annual rainfall in central Benin to MCSs and OCSs. Analysing the 2A23 product of TRMM-PR, it is interesting to note that around 36% of the produced rainfall by WCCs, DWCs and BSRs together are of stratiform nature (stratiform rainfall fractions are denoted as black framed bars in Figure 4a) and even over 50% when considering BSRs alone. This stresses the overall importance of stratiform rainfall of mature MCSs not least since this portion of the convective cloud may take several hours to overpass a region (Fink et al., 2006; Dezfuli et al., 2017). The difference in rainfall production of WCCs, DWCs and BSRs between the Coast and the Soudanian region is mainly balanced by the contribution of STRs with 37% in the Coast region down to 21% over the Soudanian region. This category, representing smaller-sized and only moderately deep convective cores, is the most frequent category across SWA and their preponderance in the coastal stripe suggests their association with afternoon land/sea-breeze convection. Despite their high frequency, ISEs and MODs together contribute only 3–7% to total rainfall.

The ratio between the integrated surface rainfall and the number of occurrences is shown in Figure 4b, which is a simple measure to compare the rainfall production per event across the categories. It is normalized based on the lowest value, which for ISEs is in the Soudanian region. As expected, BSRs produce the largest integrated rainfall amount per event among the different rainfall classes in all regions. Compared to ISEs their ratios are almost three orders of magnitude higher over the Inland and Soudanian regions. In other words,

one BSR produces the same amount of rainfall as $10^3$ ISEs. It is apparent that rainfall productivity increases with horizontal growth of convective systems but also with depth. Although DCCs contribute only up to 4% to total rainfall in SWA (Figure 4a), they are capable of producing around 10% of the rain of a BSR on average. The productivity of WCC, DWC and BSR over the Coast region is reduced compared to the other regions but this does not necessarily indicate a lower intensity. Due to the smaller north–south extent of the Coast region there is a limitation on how much a mature convective system can contribute to the total rainfall amount.

## 5.2 | Diurnal and seasonal cycles

The occurrence of the different rainfall types exhibits a distinct annual cycle. Figure 5 shows region-dependent seasonal cycles of the occurrence frequency of the rainfall categories with respect to their total number in each region. The following patterns are worth noting:

- ISEs are predominantly a phenomenon during the Sahelian phase, peaking in August in all regions (Figure 5a). The sharpness of the annual cycles grows from south to north and a jump from 5% to 20% from June to July is visible for the Inland and Soudanian regions, which marks the sudden northward progression of the WAM. A jump of this magnitude is not seen for the Coast, where the profile exhibits a gradual rise and decline before and after August, respectively.
- For MODs and STRs (Figure 5b,c) a weakly bimodal distribution in the Coast region transforms into a single-peak mode in the Soudanian region. This is similar to the mean annual cycle in Figure 3. Over the Soudanian region, two increases can be identified. The number of identified systems first increases during the coastal phase and then plateaus in June, followed by a sudden jump at the beginning of the Sahelian phase. The first increase may be related to the passage of the Intertropical Front (ITF), which eventually leads to an overall moister environment. As for ISEs, the second increase is clearly linked to the sudden northward shift of the WAM rainbelt.
- Convective systems that grow very deep (DCCs, DWCs) occur predominantly during the coastal phase (Figure 5d,f). The northward progression of maximum occurrence during the early rainy season is clearly visible. Apparently, one to two months are needed to create favourable environmental conditions for deep systems between the Coast and the Soudanian zone. Into the Sahelian phase, deep systems vanish almost completely over the Coast and Inland regions and re-appear during the retreat phase, but are then less numerous. The numbers in the Soudan region gradually decrease towards the beginning of the oceanic phase in November.
- For WCCs, the bimodal cycles for the Coast and Inland regions show a strong similarity both in peak positions
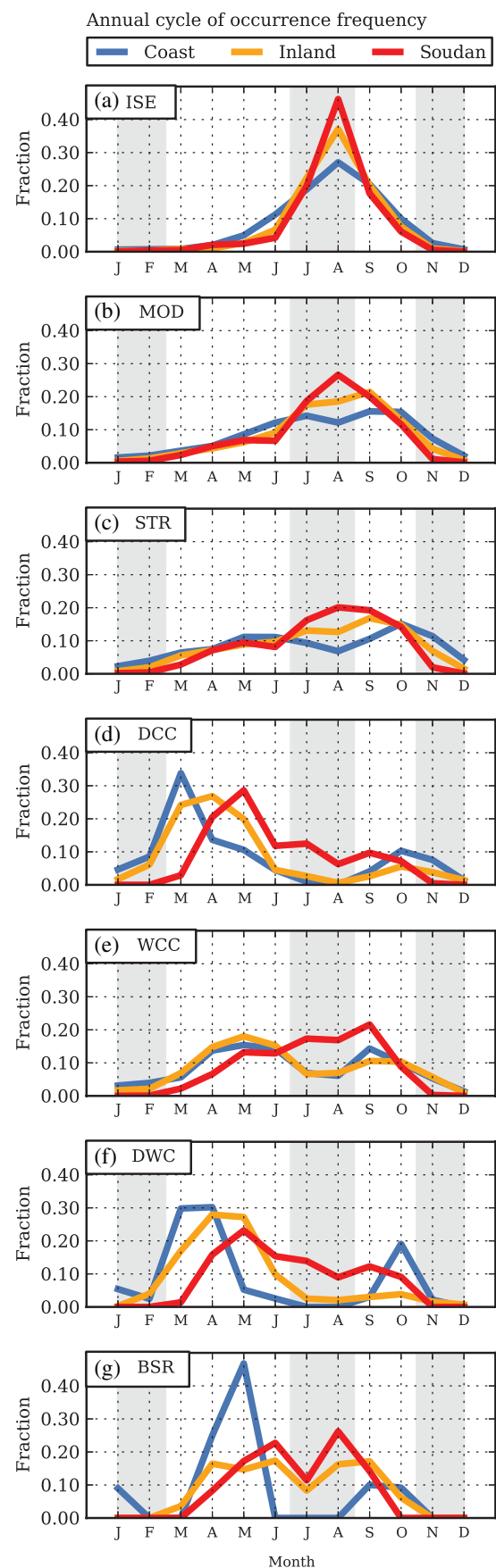


**FIGURE 5** Mean annual cycle of the fractional occurrence for each rainfall category in each subregion. The shadings again denote different phases of the rainy season over SWA (as in Figure 3) [Colour figure can be viewed at wileyonlinelibrary.com]

(May and September) and magnitude (Figure 5e). Unlike for deep systems, the conditions for larger organized convection appear to be uniform over a wider region throughout the year. In the Soudanian region, the growth in numbers is faster during the coastal phase but peaks in September. Interestingly, this peak coincides with the secondary peaks over both Coast and Inland.

- The profile for BSRs is bimodal in all regions due to a drop in July (Figure 5g). While the Coast region exhibits a marked primary peak during the coastal phase, the magnitude of the peaks over the Inland and Soudanian regions are similar. During the late Sahelian and retreat phases the occurrence frequency peaks progressively later going southward.

Figure 6 depicts the diurnal cycle of the number distribution including the location of the maxima based on harmonic analysis (denoted as dashed vertical lines). In general, the more intense and organized convective systems are, the more they are shifted into night-time. While MODs, STRs and DCCs typically occur in the afternoon and early evening, WCCs and BSRs appear in the late evening and past midnight, respectively. On average, this reflects the lifetime of fully developed MCSs that are initiated in the afternoon, organize in the evening when conditions are favourable and survive during the night owing to their self-sustaining abilities. This was found in a similar fashion by earlier studies of e.g. Mathon and Laurent (2001), Fink and Reiner (2003), Laing *et al.* (2008) and Zuluaga and Houze (2015), who investigated the occurrence of different convective systems for the Sahel. The self-sustainment and thus longer lifetime of WCCs and BSRs is also reflected in their flat diurnal profiles, indicating that these systems are less bound to the diurnal cycle once they have formed. While the distributions over the Inland and Soudanian regions are quite similar, convective systems in the Coast region develop around 2 h earlier with ISEs predominantly appearing even before noon. The latter may explain the enhanced pre-noon rainfall probability that was found at the Benin coast based on rain-gauge recordings (Fink *et al.*, 2008). Similarly, using continuous geostationary-based cloud property retrievals from SEVIRI, Young *et al.* (2018) found the highest frequency of warm rain along the coastline around midday. At the Coast, the frequency of WCCs already peaks in the early afternoon, which is partly caused by coastal convection forming a contiguous line with strong radar echoes (not shown). The land/sea-breeze circulation likely acts as a trigger for convective systems to overcome convective inhibition and to develop earlier during the day than in the regions farther north.

# 6 | ENVIRONMENTAL CONDITIONS AROUND RAINFALL EVENTS

In this section, the environmental conditions in which the convective systems grow and propagate are described. This
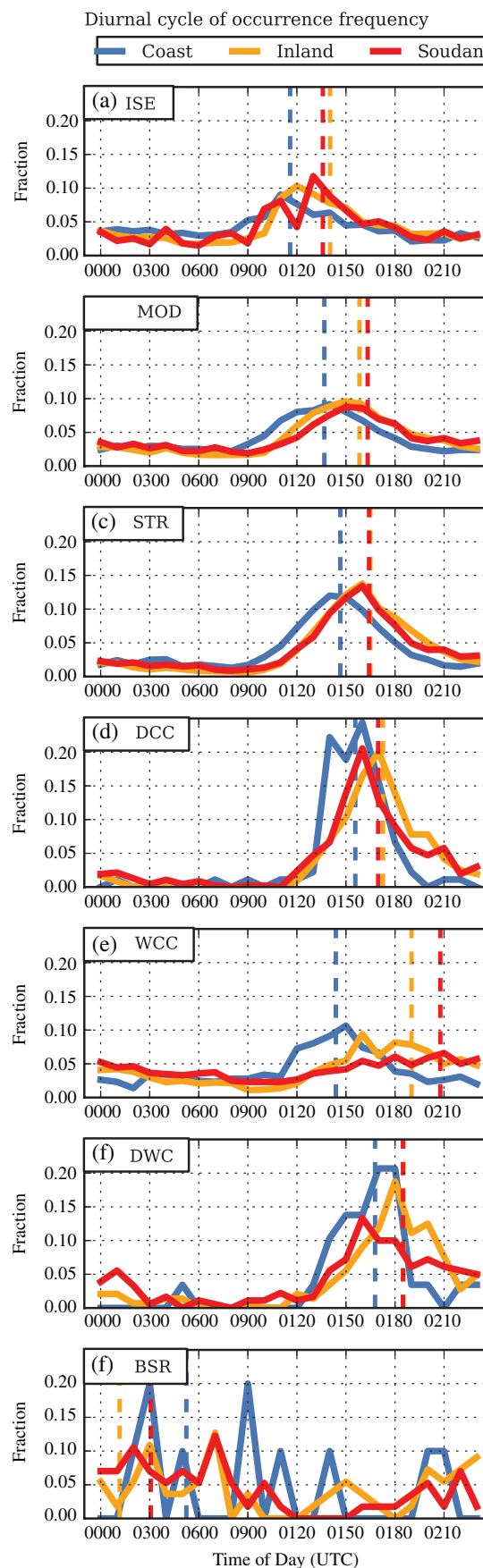


**FIGURE 6** As Figure 5, but for mean diurnal cycles. The vertical dashed lines denote the phase of the diurnal harmonic for each curve, i.e. the time of maximum occurrence, calculated through discrete Fourier transformation [Colour figure can be viewed at wileyonlinelibrary.com]
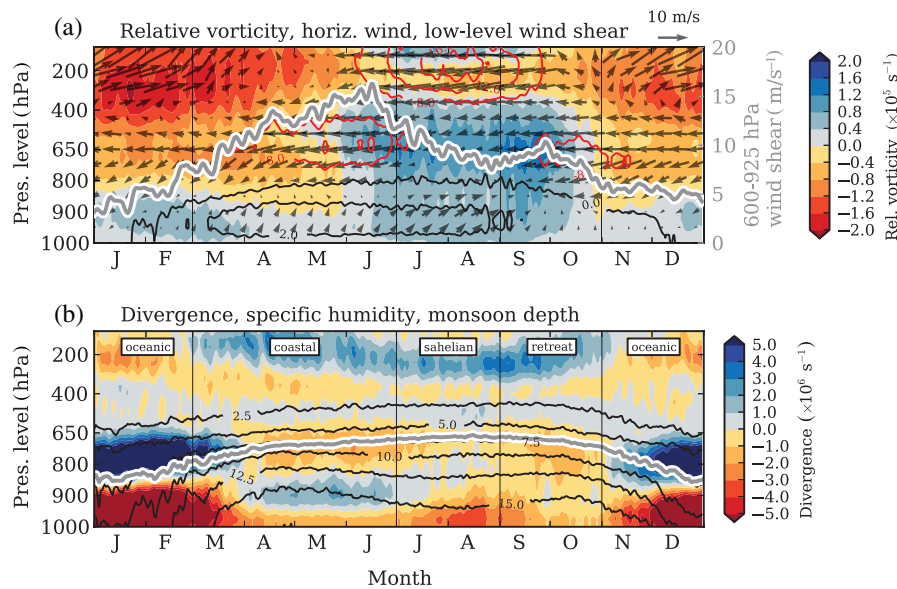
**FIGURE 7** Climatologies of seasonally varying environmental conditions. (a) Annual cycle of the vertical profile of relative vorticity (colour shading), speed and direction of the horizontal wind (arrows) and the 600–925 hPa wind shear (grey curve, m s$^{-1}$). The red contours denote strong easterlies (lower than $-8$ m s$^{-1}$) with an interval of 4 m s$^{-1}$. The black contours highlight a well-established southerly monsoon flow with an interval of 2 m s$^{-1}$ in the layer up to 700 hPa. (b) Annual cycles of the vertical profile of divergence (colour shading), the specific humidity (black contours, interval 2.5 g kg$^{-1}$) and the monsoon layer depth (grey curve). The latter is calculated after Lafore *et al.* (2017a). All quantities are based on ERA-Interim data averaged from 1998 to 2013. The thin vertical black lines denote the transition between the phases of the rainy season (as in Figure 3), which are labelled in (b) [Colour figure can be viewed at wileyonlinelibrary.com]

is preceded by a discussion of the mean annual cycle of factors known to be related to the degree of convective organization.

## 6.1 | Mean seasonal cycle

To investigate the (thermo-)dynamic factors leading to rainfall events, we first adress the underlying conditions from a seasonal perspective. A zonally averaged annual cycle of the vertical profiles of relative vorticity and horizontal wind based on ERA-Interim data is shown in Figure 7 as a time–height diagram. The zonal average was taken from 10°W to 10°E at 8°N (white dashed line in Figure 1) and thus represents the Inland region. Early in the year, the transition from the oceanic to the coastal phase is roughly marked by the change from weak northeasterlies to the southwesterly monsoon flow at lower levels (Figure 7a) with the meridional component (black contours) staying above 2 m s$^{-1}$ until the end of the Sahelian phase. During the latter, the monsoon flow gains more westerly momentum (see vectors at low-levels during July and August) and also extends to higher levels. In the mid-troposphere around 650 hPa, the occurrence of the AEJ is denoted with red contours (i.e. zonal wind $< -8$ m s$^{-1}$) during the coastal and the retreat phase. During the Sahelian phase, the AEJ moves out of the domain and is located at around 15°N. This seasonal north–south meandering of the AEJ is accompanied by a change of sign in the mean field of relative vorticity, owing to the change from the anticyclonic to the cyclonic shear side and back. The first AEJ passage also marks the period of highest 600–925 hPa vertical

wind shear with over 15 m s$^{-1}$ in mid-June. Vertical wind shear is considered to be a key factor for the organization of shear-perpendicular convective elements (e.g. Sultan and Janicot, 2003; Nicholls and Mohr, 2010; Taylor *et al.*, 2017). It decreases during the Sahelian phase down to around 8.5 m s$^{-1}$ and slightly regains strength during the second passage of the AEJ in the retreat phase (up to 10 m s$^{-1}$). Strong easterlies are also found in the upper troposphere related to the Tropical Easterly Jet (TEJ), which peaks during the Sahelian phase.

The change of the low-level flow is also evident in the divergence and humidity fields (Figure 7b). During the oceanic phase, convergence prevails in the layer up to 900 hPa with corresponding divergent motions aloft. It marks the period of the shallow meridional overturning in the region of the ITD at the surface and the anticyclonic shear side of the AEJ aloft (Nolan *et al.*, 2007; Zhang *et al.*, 2008). With the onset of the monsoonal southwesterlies, the specific humidity at low levels rises quickly to over 15 g kg$^{-1}$. It decreases during the Sahelian phase and briefly rises in the retreat phase. During the period of higher specific humidity between March and October, divergent flow is also found at the 200 hPa level in accordance with the onset of a higher frequency of deep convection (Figure 5). The seasonal variations in specific humidity decrease with height. The development of the monsoon layer (grey curve), a thermodynamic measure for the depth of humid air in the monsoon (Lafore *et al.*, 2017a) based on precipitable water (PW), shows a rather gradual increase in height towards the Sahelian phase and a decrease in the retreat phase. The curve roughly follows the 7.5 g kg$^{-1}$ contour of specific humidity.
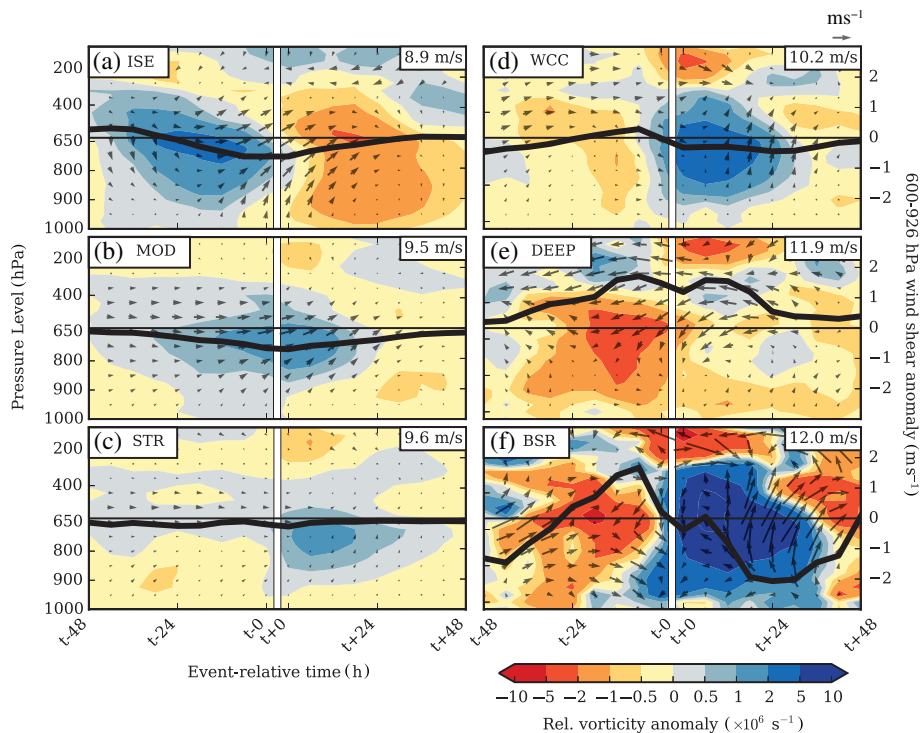
**FIGURE 8** Composited time–height ERA-Interim profiles of the anomalies of relative vorticity (colour shading) and of horizontal wind speed and direction (arrows) in a ±48 h period around the passage (vertical white line) of a convective system belonging to a given rainfall category at gridpoints selected as described in section 6.2. t±0 represent the closest timesteps before and after the onset of the event, respectively. The anomalies were determined by subtracting the values at the actual event from their respective 1998–2013 means. Numbers denoting the mean background absolute wind shear for the rainfall types are given in the top right corner of the panels. The thick black curves denote the anomaly of the 600–925 hPa vertical wind shear (m s$^{-1}$). The thin horizontal black line is the zero line for the wind shear anomaly. Information from DCC and DWC are combined in (e) [Colour figure can be viewed at wileyonlinelibrary.com]

## 6.2 | Results for TRMM-PR-based rainfall types

The local development of the environmental conditions in a 4-day window around the rainfall events is analyzed in Figures 8 and 9 based on anomalies from six-hourly mean profiles of ERA-Interim. These mean profiles are based on the 1998–2013 period. For the calculation of the anomalies, all profiles in the 4-day window were taken from the closest ERA-Interim gridpoint to the position of the convective system in TRMM-PR and were eventually subtracted from the respective mean profiles. Note that the positions of the rainfall systems were determined by their centre of gravity, which means that the leading portion of the rainfall area may have arrived earlier at a gridpoint, specifically for larger systems such as BSRs. For the purpose of a condensed analysis, Figures 8 and 9 show composites over all subregions combined. In essence, the structures of the anomaly fields are mostly comparable between the subregions but their magnitudes differ. While we refer to the File S1 for a more detailed discussion, important regional differences will be mentioned in this section.

Figure 8 shows the evolution of the anomaly fields of relative vorticity, the anomaly of the horizontal wind expressed as arrows and the anomaly 600–925 hPa wind shear denoted as black curves. Additionally, the climatological background values of low-level wind shear determined by the mean fields described above are indicated in the top right corners. For

this analysis, information from the deep core categories DCC and DWC are combined into DEEP, as no substantial differences were found between them with respect to the anomaly fields. It is evident that rainfall events over SWA generally occur in connection with mid-level vorticity disturbances. ISEs and MODs develop under distinct westerly to southwesterly wind anomalies at mid-levels (Figure 8a,b). They appear to be linked with a cyclonic anomaly that acts to reduce the lower tropospheric wind shear. Note that the respective background low-level wind shear is already lowest among all categories (8.9 and 9.5 m s$^{-1}$, respectively), which suggest that less intense convection favourably occurs in a weakly sheared environment. In the case of ISEs, such a regime is established between a deep dipole configuration of a preceding cyclonic and a succeeding anticyclonic anomaly. One can assume that this and the wave-like pattern of the wind anomalies reflect the passage of a mid-tropospheric wave, most likely but not exclusively an AEW. ISEs develop predominantly on the eastern flank of the wave trough. Such a dipole configuration is absent in the case of MODs which predominantly develop during the passage of a single cyclonic disturbance. This regime may occur on the southern flank of the cyclonic anomaly where the usually prevailing mid-tropospheric easterlies are weakened the most. However, the effect of reduced low-level wind shear decreases towards the region ahead of the cyclonic anomaly and enables the occurrence of more intense rainfall
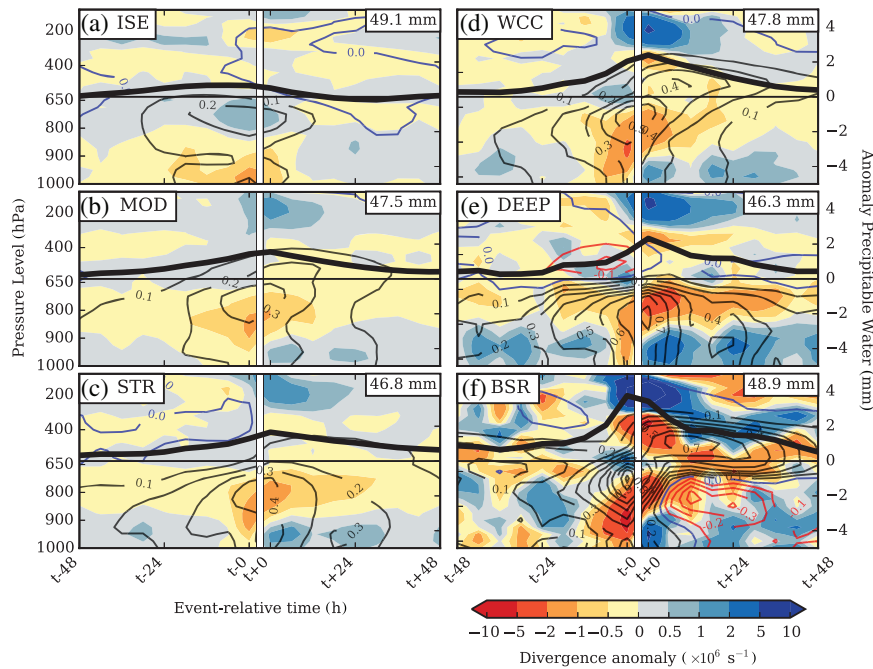
**FIGURE 9** As Figure 8, but for the anomalies of divergence (colour shading), of specific humidity (contours) and of precipitable water (PW, thick black curve). For the specific humidity, positive contours appear as black and negative values as red, with 0.1 g kg$^{-1}$ interval, and the blue contour denotes the zero line. The mean background PW for the rainfall type is given in the top right corner of each panel. Information from DCC and DWC are combined to in (e) [Colour figure can be viewed at wileyonlinelibrary.com]

systems, as can be inferred from the profile of STRs where anomalies in the horizontal flow are weak (Figure 8c). Organized convection (WCCs, BSRs; Figure 8d,f) occurs ahead of a cyclonic and behind an anticyclonic vorticity anomaly. Westerly wind anomalies at mid-levels prior to the event are suppressed and turn to southerly directions. The influence of this vorticity dipole on the vertical wind shear is clearest for BSRs (Figure 8f), where the passage of the anticyclonic (cyclonic) vortex strongly enhances (reduces) shear. That said, BSRs develop predominantly during periods with a large background shear (12 m s$^{-1}$). In the case of DEEP (Figure 8e), anticyclonic signals at mid-levels precede the event, accompanied by northeasterly anomalies and thus increased low-level vertical wind shear. However, the structure of a cyclonic anomaly is less pronounced. This profile is in stark contrast to those of MODs and STRs (Figure 8b,c).

The distinct dipole structure of the anomaly field of relative vorticity around BSR events is typical for the Soudanian region but becomes less pronounced towards the Coast region (File S1). In fact, BSRs in near coastal areas tend to occur closer to the centre of the cyclonic disturbance while the vorticity dipole vanishes at the same time. In a similar although less striking fashion, the occurrence of ISEs is drawn towards the cyclonic centre over the Soudanian region. These distinctive differences of the environmental conditions for convective systems on the opposite side of the intensity spectrum indicate where favourable conditions for organized convection are created by mid-level disturbances in different regimes.

In Figure 9, controlling factors for rainfall at lower levels are analyzed through the anomaly fields of divergence (shading), the moisture field (contours) as well as the anomaly in PW (black curve). The background values of PW are presented in the top right corners. We note that some uncertainties with respect to these three quantities have to be taken into account; since the evolution of both mass and moisture budgets is governed, amongst other things, by precipitation (e.g. Berrisford *et al.*, 2011), the representation of the respective fields depends on the ability of ERA-Interim to resolve the rainfall systems. Nonetheless, coherent signals of low-level convergence just ahead of the passage of any rainfall category prevail and coincide with an increase of both positive specific humidity and PW anomaly, all strongest in the case of BSRs (Figure 9f). This indicates that local moisture convergence plays a substantial role for the establishment of organized convection. However, from the perspective of absolute values, PW is not a suitable predictor for rainfall types. For instance, the environment around low-intensity ISE events (Figure 9a) exhibit the highest background value of PW among all categories (49.1 mm). Therefore, for the more humid SWA, it can be assumed that a redistribution of existing moisture through low-level convergence/divergence has a higher impact on the evolution or occurrence of certain rainfall types than the mere availability of moisture itself. Finally, we briefly note that ERA-Interim is able to capture large convective systems, such as a BSR. After its passage, a vertical dipole structure in the anomaly field of specific humidity is found with drying in the lower troposphere and a layer of ongoing moistening aloft (Figure 9f). This is the widespread trailing stratiform region
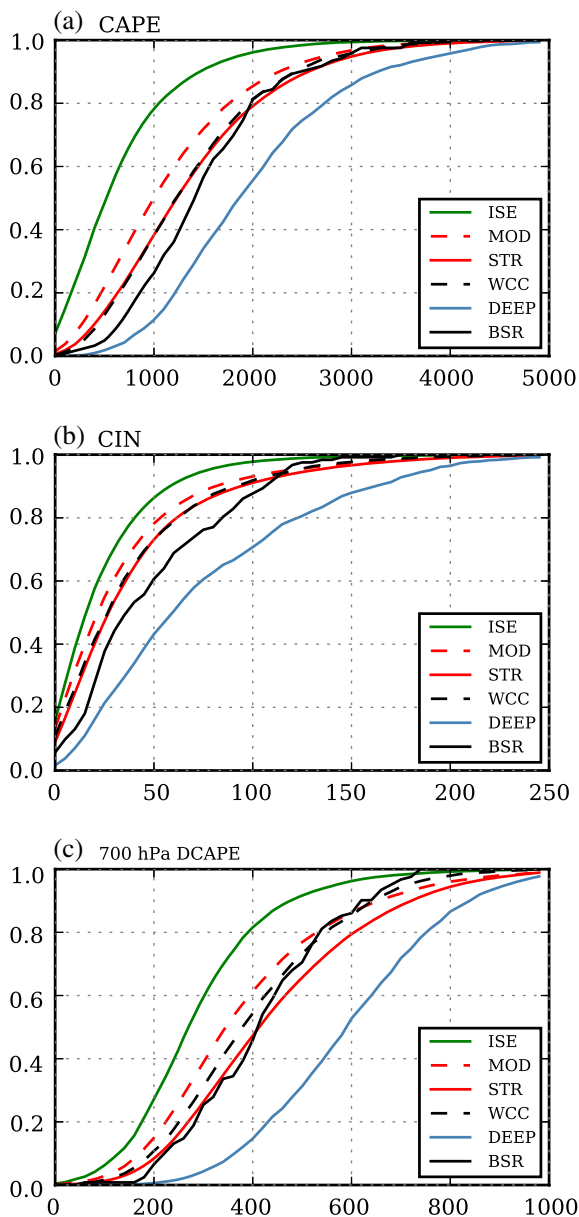
**FIGURE 10** Cumulative distribution function of (a) CAPE, (b) CIN and (c) 700 hPa DCAPE in J kg$^{-1}$ for each rainfall category. The respective value ranges were divided into 50 bins, resulting in an interval of 100 J kg$^{-1}$ for CAPE, 5 J kg$^{-1}$ for CIN and 20 J kg$^{-1}$ for DCAPE. Data from DCC and DWC are combined in DEEP [Colour figure can be viewed at wileyonlinelibrary.com]

of the BSRs. The overall structure is in accordance with the post-OCS radiosonde profile in Fink *et al.* (2006) which exhibits a drying (moistening) of the low (mid to upper) levels.

It should be stressed here that the environmental conditions shown in Figures 8 and 9 are bulk means. In fact, pre-storm conditions for all rainfall categories exhibit large variations specifically with respect to the magnitudes of vertical wind shear (cf. Nicholls and Mohr, 2010) and low-level divergence which are masked out in the composites. Some more details on the variability of the environmental controls across the rainfall classes are presented in the File S1. In a similar fashion, the thermodynamical controls prior to the rainfall

event show a wide range of values as indicated in Figure 10 which shows the cumulative distribution function of the (lowest 100 hPa based) CAPE, convective inhibition (CIN) and 700 hPa based downdraught CAPE (DCAPE) averaged over the 24 h period before the onset of the events. DCAPE quantifies the potential acceleration of an air parcel cooled by evaporation when it descends pseudo-adiabatically towards the surface. Thus, it can serve as an estimator for the strength of a cold pool and the potential degree of self-sustainment of an MCS. It shall be stressed that the purpose of comparing ERA-Interim-derived convective indices is to highlight differences in the thermodynamic fields among the rainfall categories. Since these indices are generally influenced by model numerics and parametrizations in analysis products (Molini *et al.*, 2011), the focus here is more on comparison between rainfall categories and less on absolute values. All three thermodynamical variables are log-normally distributed which reflects the highly variable conditions under which the rainfall categories of different degrees of organization occur. However, with respect to the overall representation of the curves, three distinct groups can be identified: First, ISEs stand out exhibiting the lowest median values in CIN ($-20$ J kg$^{-1}$), CAPE (618 J kg$^{-1}$) and DCAPE values ($-290$ J kg$^{-1}$). Such low CAPE and CIN conditions are known to be prevailing over the ocean (Riemann-Campe *et al.*, 2009). As such, ISEs form in a moisture-laden troposphere (background value of PW in Figure 9a), which explains the maximum frequency in the Sahelian phase in all regions. As seen in Figure 8 it is established through deep southwesterly anomalies before the event. The second group contains MODs, STRs, WCCs and BSRs. The group median values are $-29$ J kg$^{-1}$ for CIN, 1,222 J kg$^{-1}$ for CAPE and $-398$ J kg$^{-1}$ for DCAPE. The fact that this group includes categories of varying intensities and degree of organization implies that the magnitude of the thermodynamic variables are of lesser importance for the higher organized categories WCC and BSR, particularly if cold-pool dynamics start dominating the initiation process of new convective cells. This is also evident in Fink *et al.* (2006) where no clear relationship between rainfall type and the magnitude of radiosonde-derived convective indices before the rainfall event was evident. The third group is formed by DEEP (DCCs + DWCs) which exhibits the highest median CIN, CAPE and DCAPE values (CIN: $-64$ J kg$^{-1}$, CAPE: 1,962 J kg$^{-1}$, DCAPE: $-610$ J kg$^{-1}$). As DEEP are predominantly phenomena during the coastal phase, this reflects the conditions during that stage of the WAM season. Composite vertical profiles from ERA-Interim of temperature and dewpoint temperature reveal that higher DCAPE is caused by the presence of drier air at mid-levels (cf. Figure 9d,f), while the higher values of CIN and CAPE are due to drier and warmer low levels, respectively (not shown). Therefore, moisture convergence is crucial as it acts to lower CIN (not shown) while high CAPE explains the deep nature of DCCs and DWCs.
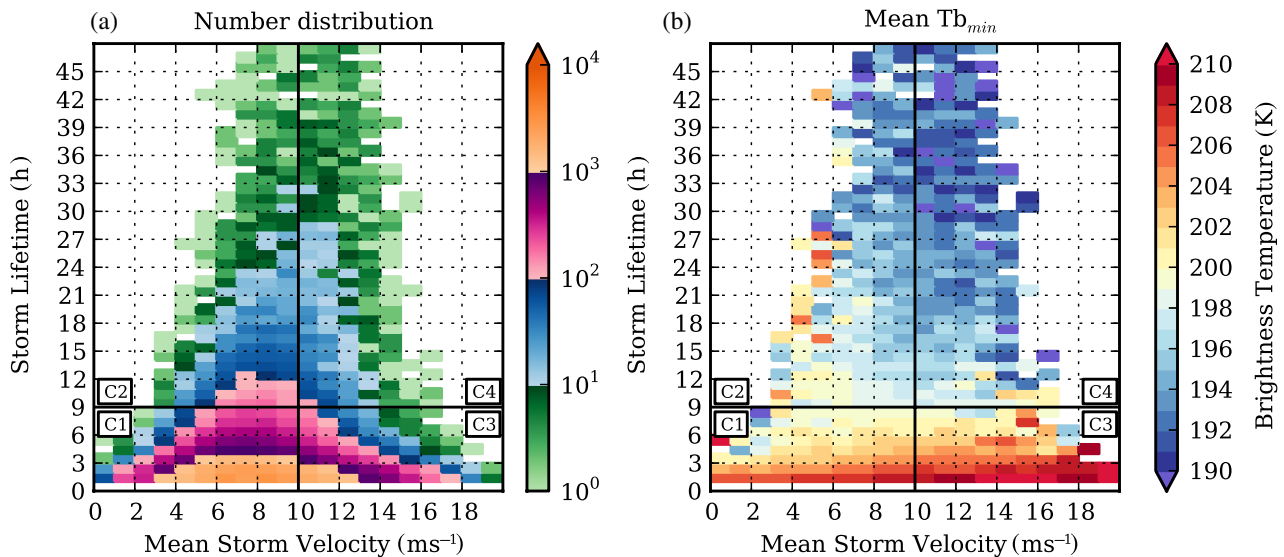
**FIGURE 11** 2D histograms of (a) the number of convective systems in relation to their mean translation speed (abscissa, m s$^{-1}$) and their lifetime (ordinate, h) and (b) the minimum brightness temperature ($Tb_{min}$) of the cloud top averaged over the whole lifetime for each bin. Convective elements were detected through the tracking routine described in section 3 which was applied on the IR dataset of SEVIRI for the period 2004–2013. Note that convective systems originating from a split or ending up as a merger are not included to avoid contamination of the distribution with respect to lifetime. Furthermore, only convective systems with a lifetime >1 h are presented. Only the first 48 h of lifetime are displayed. The convective systems are classified into four groups after Lafore *et al.* (2017b): short-lived (i.e. <9 h lifetime) and slow systems (i.e. <10 m s$^{-1}$) as C1, long-lived and slow systems as C2, short-lived and fast systems as C3 and fast, long-lived systems as C4 [Colour figure can be viewed at wileyonlinelibrary.com]

# 7 | LINK BETWEEN TRMM-PR AND IR-BASED RAINFALL TYPES

Since TRMM-PR provides only snapshots, no further information about the life-cycle of the observed convective systems can be extracted. Up to this point, all rainfall systems in the TRMM-PR have the same lifetime, i.e. 1 h, and thus do not develop from or into one of the other categories. The advantage of IR imagery is its ability to continuously observe cloud features and their development with high spatial and temporal resolutions, but it suffers, in turn, from a high uncertainty in rainfall estimation as pointed out in section 1. Thus, we attempt in this section to shed light on the question of how the categories defined on the basis of TRMM-PR are related to existing IR-based classifications of convective systems.

An overview is given in Figure 11a, which shows a two-dimensional histogram of convective systems with respect to the mean storm velocity and lifetime. Here, only those systems were included that intersected the domain from 4 to 12°N and 10°W–10°E and that underwent a clean life-cycle of at least 1 h, i.e. no splitters or mergers by definition (section 3). We first apply the IR-based classification of Lafore *et al.* (2017b). The sample is split into four classes: C1 are short-lived (i.e. <9 h lifetime) and slow systems (i.e. <10 m s$^{-1}$) and C2 are long-lived and slow. Accordingly, C3 are short-lived but fast-moving while C4 are fast, long-lived systems. It becomes evident that the majority of convective systems over SWA exhibit a rather short lifetime. Around 94% belong to the short-lived classes C1 + C3. However the storm velocities are quite variable and can reach up to 20 m s$^{-1}$. Overall, the average velocity is around

8.2 m s$^{-1}$. As the lifetime of convective systems increases, there is a clear lower and upper limit for the storm velocity at which such systems propagate. For systems with a lifetime >24 h, there are very few systems propagating slower and faster than 5 and 15 m s$^{-1}$, respectively. The latter value is comparable to highly organized systems in the Soudanian and Sahelian region, where systems move at an average speed of 12–13.5 m s$^{-1}$ (Mathon and Laurent, 2001; Fink *et al.*, 2006), and in some cases even faster than 15 m s$^{-1}$ (Schrage *et al.*, 2006). Considering the classes of long-lived systems (C2 + C4), we find an average speed of 9 m s$^{-1}$ and 10.3 m s$^{-1}$ for those with a lifetime of >24 h. From Figure 11b, which shows the mean lifetime-spanning minimum brightness temperature ($Tb_{min}$) of the cloud top for each bin, a relationship between lifetime and $Tb_{min}$ becomes evident. Cloud-top temperatures of very long-lived systems (>24 h) can drop lower than 190 K, while the average temperatures gradually increase for shorter lifetimes. Systems within C1 and C3 rarely exhibit $Tb_{min}$ lower than 200 K on average. These long-lived systems typically originate in the proximity of elevated terrain and are found in higher numbers during the coastal and retreat phases of the WAM (not shown).

Table 1 summarizes the assignment of the TRMM-PR rainfall categories to the aforementioned IR-based classification. Being warm cloud systems by definition (i.e. cloud-top temperatures above freezing), ISEs are excluded from this analysis as such clouds were not tracked. In addition, some systems of the other categories were not incorporated in the analysis for two reasons. First, splitters and mergers are not considered. The percentage of convective systems that were omitted for this reason is denoted as "Split and/or merge" in

**TABLE 1** Assignment of TRMM-based rainfall categories to IR-based categories C1–C4, as defined by Lafore *et al.* (2017b). For details see text and Figure 11

| TRMM-PR category | C1 | C2 | C3 | C4 | Sample size | No label | Split and/or merge | Avg. speed (m s⁻¹) |
|---|---|---|---|---|---|---|---|---|
| BSR | 0.0% | 30.8% | 0.0% | 69.2% | 65 | 0% | 38% | 10.6 |
| DWC | 12.2% | 35.6% | 2.6% | 49.6% | 158 | 0% | 31% | 9.9 |
| WCC | 24.3% | 38.3% | 7.8% | 29.6% | 1,538 | 3% | 36% | 9.3 |
| DCC | 40.7% | 28.7% | 10.8% | 19.8% | 376 | 6% | 21% | 8.6 |
| STR | 43.3% | 24.3% | 13.2% | 19.2% | 12,640 | 63% | 12% | 8.8 |
| MOD | 29.5% | 34.3% | 7.2% | 29.0% | 14,314 | 79% | 7% | 9.1 |

'Sample size' denotes the number of convective systems that are available from 2004 to 2013 from the TRMM-PR dataset.
'No label' indicates the percentage of 'Sample size' that was missed by the tracking routine due to unmatched temperature and/or area size thresholds.
'Split and/or merge' indicates the percentage of 'Sample size' that is omitted because it originates from a split and/or ended as a merger, both of which are not considered for Figure 11.

Table 1. A relatively high fraction (>30%) of WCCs, DWCs and BSRs originate from split and/or end their life-cycle by merging with another convective system. This fraction is lower for the less intense categories MOD and STR. Second, some systems are unassigned, as they fail to match at least one of the thresholds for area (900 km²) and temperature (233 K) of the tracking routine (denoted as "no label" in Table 1). This applies to 63% of MODs and 79% of STRs.

As expected, BSRs are purely long-lived systems (i.e. a lifetime > 9 h) and tend to be faster than $10\,\text{m s}^{-1}$ (C4 = 69.2% compared to C2 = 30.8%). Longevity is also emphasised for the wide classes WCC (C2 + C4 = 66.8%) and DWC (C2 + C4 = 84.4%). The fact that the majority of BSRs and DWCs belong to the faster category reflects their typical environment with high vertical wind shear (Figure 8). For shear-perpendicular linear systems, such as squall lines, high vertical wind shear is known to be crucial for the generation of new cells on the downshear side of the systems (e.g. Rotunno *et al.*, 1988) and effectively leads to a higher translation speed. We note that this does not hold for shear-parallel systems and/or nonlinear systems (e.g. Nicholls and Mohr, 2010) which might be represented by

the slower category C2. From Table 1, the mean velocity of MCS-like categories ranges from 9.3 to $10.6\,\text{m s}^{-1}$. STRs and DCCs are predominantly slow systems (C1 + C2 is 66.4% and 68.9%, respectively) whereas, interestingly, 63.4% of MODs are assigned to long-lived convection. However, it can be assumed that the fraction of MODs contributing to the short-lived classes C1 and C3 is higher than indicated. As mentioned above, a high percentage of the sample drops out of analysis also due to the temperature restriction of the tracking routine. The fact that short-lived systems exhibit the warmest cloud tops (Figure 11b) suggests that a larger fraction of unassigned MODs may fall into either of the categories C1 or C3. This likely also holds for STRs.

In a further analysis, the IR classification introduced in Mathon *et al.* (2002) and Fink *et al.* (2006) is applied. The authors define cloud features with a contiguous area of at least $5000\,\text{km}^2$ and a temperature of $\leq$233 K as MCSs. Furthermore, OCSs are identified if the cloud exhibits a contiguous area of $\leq$213 K exceeding $5000\,\text{km}^2$ for at least three subsequent hours. Additionally, systems must propagate at an average speed of $\geq$$10\,\text{m}^{-1}\text{s}$. The occurrence frequency of MCSs as a function of mean speed and storm lifetime is
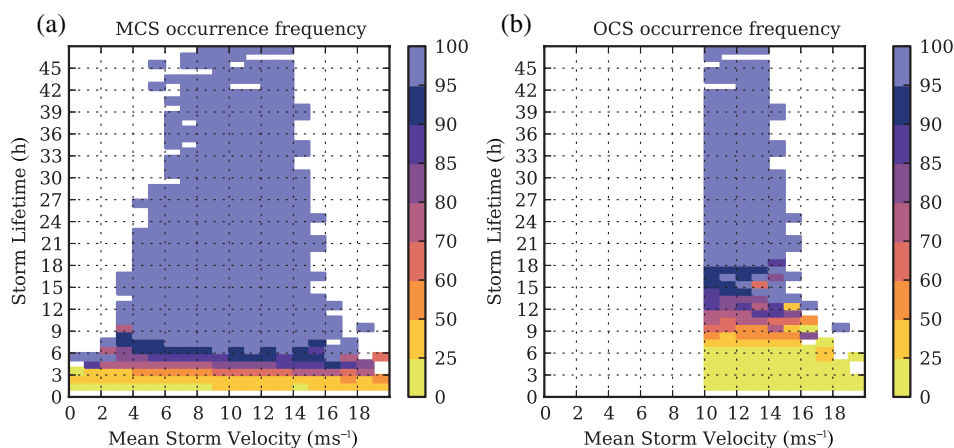


**FIGURE 12** 2D histograms for (a) the occurrence frequency of MCSs and (b) the occurrence frequency of OCSs per bin expressed in percent. The definition of MCSs and OCSs follows Mathon and Laurent (2001) and Fink *et al.* (2006). For each bin, the frequency was calculated by the number of MCS/OCS divided by the total number of convective systems in the respective bin (see Figure 11a) [Colour figure can be viewed at wileyonlinelibrary.com]

**TABLE 2** Assignment of TRMM-based rainfall categories to the IR-based categories MCS and OCS as defined in Mathon and Laurent (2001) and Fink *et al.* (2006)

| TRMM-PR category | MCS | OCS | MCS-to-OCS conversion |
|---|---|---|---|
| BSR | 100.0% | 68.2% | 68.2% |
| DWC | 100.0% | 52.2% | 52.2% |
| WCC | 96.1% | 30.2% | 31.4% |
| DCC | 93.7% | 21.6% | 23.1% |
| STR | 80.7% | 20.2% | 25.1% |
| MOD | 90.7% | 28.9% | 31.9% |

'MCS-to-OCS conversion' indicates the percentage of MCSs that eventually reached the stage of an OCS.

shown in Figure 12a. Here, the frequency is determined as the number of storms that fulfil the MCS criterion for at least one time step (i.e. 15 min) divided by the total number of identified convective systems per bin (Figure 11a). The MCS occurrence frequency depends on storm lifetime but already reaches a percentage of >90% at 6 h. Around 98% of all systems with a lifetime longer than 6 h are MCSs. In contrast, OCSs are less frequent (Figure 12b), primarily since a mean velocity of at least $10 \, \mathrm{m \, s^{-1}}$ is a necessary condition for an OCS as mentioned above. However, of all systems that exceed $10 \, \mathrm{m \, s^{-1}}$ and live longer than 6 h, only around 66% reach the stage of an OCS. The 90% mark is reached around a storm lifetime of 14 h. Around this value, there is a slight tendency for more OCSs with faster propagation. This supports the suggestion that a strongly sheared environment, which is assumed to be associated with faster propagation of convective clouds (e.g. Fink *et al.*, 2006), favour the development of highly organized systems (Schrage *et al.*, 2006).

In Table 2, the fraction of the TRMM-PR categories fulfilling the definition of MCSs and OCSs is presented. Generally, the fraction of systems that become MCSs at one point during their lifetime is high. Not surprisingly, all the BSRs and DWCs reach the MCS stage. The fraction is lowest for STRs at 80.7%. The fact that MODs exhibit a higher value than STRs may again be a reflection of the sampling issue for MODs that became evident in Table 1. The percentage of systems becoming an OCS is substantially smaller than that for MCS for every TRMM-PR category. Again, BSRs and DWCs exhibit the highest fraction with 68.2 and 52.2%, respectively. For WCCs the fraction already drops to 30.2%. The major limiting factor in this context is the velocity threshold of $10 \, \mathrm{m \, s^{-1}}$ for OCSs, which is only exceeded by BSRs on average (Table 1). Nonetheless, for WCCs, rather less than a third of all MCSs become OCSs (31.4%). This MCS-to-OCS conversion rate is lowest for DCCs and STRs at 23.1% and 25.1%, respectively.

## 8 | SUMMARY AND DISCUSSION

In a novel approach, we combined the TRMM-PR, ECMWF reanalysis and Meteosat IR datasets to explore the rainfall characteristics over SWA from a climatological perspective. The necessity for such an extensive rainfall analysis over the understudied SWA is underpinned by the fact that the skill of quantitative rainfall predictions on short and long time-scales is still poor in climate projections and operational forecasting (Christensen *et al.*, 2013; Vogel *et al.*, 2018) in this region. Much of this has resulted from a lack of understanding of (a) the composition of different rainfall systems that contribute to total rainfall, (b) the environmental controls under which the systems occur and (c) the implication of these conditions for the life-cycle of convective systems. The results of these three points are summarized in the following. Regarding the environmental conditions, we note that we focused on the analysis of their bulk means throughout this article. In the File S1 a more detailed discussion about the spatio-temporal variability of both rainfall types and environmental controls is provided.

### 8.1 | Contribution of different rainfall types to total rainfall amount

Our results have shown that the majority of rainfall over SWA is provided by MCS-type rainfall systems with extensive convective and stratiform regions, although they are considerably outnumbered by smaller and less-intense rainfall types. There is a latitudinal dependence with the relative contribution of MCSs to total rainfall decreasing southward (71% in the Soudanian region to 56% at the coast), while the contribution of weaker convective systems increases. Typically, these less-intense rainfall systems are phenomena which occur predominantly in the afternoon, whereas the MCS types organize later in the evening and mature during the night. The general implication of these findings is that the frequency of MCSs crucially determines the magnitude of annual rainfall. However, their importance is progressively reduced towards the moister coastal region where non-organized, diurnal convection becomes more and more significant. This latitudinal dependence of the composition of rainfall has already become evident from earlier independent analyses with ground-based rainfall measurements. Local thunderstorms, likely STRs in this study, dominate the rainfall fraction at the coast (Acheampong, 1982; Omotosho, 1985), whereas the contribution of long-lived, organized convective systems is largest in the Soudanian zone farther north (Omotosho, 1985; Fink *et al.*, 2006). From a climatological perspective, we can generally confirm these findings where the main constraints of the previous studies have been the short investigation periods and the too localized scope to translate their results to the entire SWA. Having based this analysis on randomly distributed TRMM-PR snapshots in space and time, we note again that successive TRMM overpasses may observe the same convective system during different stages. As such, both number and rainfall distributions potentially contain contributions from the same rainfall systems but, given the TRMM PR space–time sampling, this should not significantly affect the results.

**TABLE 3** Qualitative summary of the (thermo-)dynamical conditions during the passage of the TRMM-PR based rainfall categories, sorted by their rainfall production after Figure 4b from low to high. The AEW phases were taken from e.g. Reed *et al.* (1977) and Janiga and Thorncroft (2016)

| No. | Category | Wind shear | CAPE | CIN | DCAPE | Possible AEW phase (Coast/Inland/Soudanian region) |
|---|---|---|---|---|---|---|
| 1 | ISE | Low | Low | Low | Low | 7/6/5 |
| 2 | MOD | Low | *Medium* | *Medium* | *Medium* | — |
| 3 | STR | *Medium* | *Medium* | *Medium* | *Medium* | — |
| 4 | DCC | **High** | **High** | **High** | **High** | — |
| 5 | WCC | *Medium* | *Medium* | *Medium* | *Medium* | 3/2/2 |
| 6 | DWC | **High** | **High** | **High** | **High** | — |
| 7 | BSR | **High** | *Medium* | *Medium* | *Medium* | 4/3/2 |

A differentiation was made between the AEW phases for the Coast region, the Inland region and the Soudanian region, based on Figures S3–S5 in the File S1.

The present study has also highlighted the different character of rainfall at the immediate coastline compared to the regions farther inland. Not only is the fractional occurrence of shallow, pure warm-rain events highest at the coast, but the initiation of isolated diurnal convection as well as intense convective lines parallel to the coast is also shifted forward in time by around 2 h to midday and early afternoon. In a consistent manner, long-term rainfall measurements across Benin for the period 1962–1990 have shown highest rainfall probability in the morning hours at coastal stations. The rainfall probability then swiftly shifts to the late afternoon at inland stations (Fink *et al.*, 2008). Therefore, we conclude that coastal rainfall on a diurnal time-scale is dominated by the effects of land/sea-breeze interactions, promoting both typical oceanic phenomena such as shallow, warm-rain clouds through the establishment of a more maritime environment and intense coastal convection through sea-breeze convergence.

The general importance of warm-rain events to total rainfall over SWA remains uncertain. Contrary to their high numbers at the coast, our results indicate that the importance of these shallow warm-rain events with respect to total rainfall is quite low (2%). However, with respect to their definition in this study, they only comprise the isolated, convective elements below the freezing level (Schumacher and Houze, 2003). Since warm-rain processes are not only constrained to e.g. stand-alone, isolated clouds (Liu and Zipser, 2009) nor to environments with temperatures above 0 °C (i.e. supercooled clouds, e.g. Huffman and Norman, 1988), further analysis of the rainfall types is required with a refined definition of potential warm-rain areas. Possible options include a method introduced in Young *et al.* (2018) where a combination of cloud optical depth and effective radius information from SEVIRI was used to delineate these areas.

## 8.2 | Environmental conditions

In composited vertical profiles derived from ERA-Interim fields, the (thermo-)dynamic conditions and their evolution around the time of occurrence of each rainfall type were presented. The typical environmental conditions for each rainfall type defined in this study are summarized in Table 3. On that note, we stress again that the composites presented in Figures 8 and 9 conceal strong variations in the environmental controls under which the various range of rainfall categories develop over SWA. A brief discussion about this variability is compiled in the File S1.

In principle, rainfall events are accompanied by mid-level vorticity anomalies that have a direct impact at least on the low-level (i.e. 600–925 hPa) wind shear. The passage of a cyclonic (anticyclonic) disturbance coincides with decreased (increased) wind shear due to southwesterly (northeasterly) anomalies at mid-levels. These two regimes promote rainfall types on opposite sides of the intensity spectrum. A higher degree of convective organization is found in situations of enhanced shear, leading to the occurrence of MCS-type rainfall systems, particularly fast-moving squall lines as found in Schrage *et al.* (2006). In contrast, less intense convective systems typically occur in areas of suppressed wind shear under the influence of a single cyclonic disturbance. Particularly deep westerly anomalies are typically accompanied by weak but long-lasting rainfall, termed as "vortex-type rainfall" (Fink *et al.*, 2006; Schrage *et al.*, 2006).

Furthermore, the modulation of vertical wind shear was found to be particularly pronounced during the passage of an AEW or similar wave disturbances (Knippertz *et al.* (2017) gives a discussion of different types of SWA vortices). The most (least) intense rainfall types in this study (i.e. MCSs with a developed convective and stratiform region and isolated shallow echoes, respectively) are typically located in the region west (east) of the wave trough, i.e. the regime of highest (lowest) low-level wind shear. This is in line with a recent study by Janiga and Thorncroft (2016) who found more intense systems in the area of AEW maximum northerlies (N or AEW phase 2, west of the wave trough) and a larger amount of weak systems in the region of maximum southerlies (S or AEW phase 6, east of the wave trough). However, the location of mature MCSs within the wave signature and

the structure of the wave itself is region-dependent (File S1). While the aforementioned dipole structure of vorticity is typical for the Soudanian region, it becomes less pronounced in near-coastal areas. Furthermore, mature MCSs tend to occur closer to the centre of the cyclonic disturbance. Interestingly, the opposite is true for non-organized shallow convection whose occurrence is drawn closer to the cyclonic disturbance over the Soudanian region. This latitudinal region dependence for favourable conditions of organized convection in coastal and continental regimes over West Africa has already been mentioned in early studies (e.g. Aspliden *et al.*, 1976; Duvel, 1990) and also draws comparisons to the oceanic-continental regimes described in Janiga and Thorncroft (2016).

On an interesting note, there also seems to be a longitudinal dependence over West Africa. Guy *et al.* (2011) analysed MCSs and the respective environmental conditions over 29 days and three different regimes of West Africa (maritime, coastal and continental) based on radar and sounding observations aligned around 15°N. In this study, MCSs tend to occur equally ahead of and behind the AEW trough, while they are mostly found ahead of the trough in the continental regime. It indicates a certain dependence on the proximity to the coast, probably coinciding with a change in the strength of vertical wind shear. How the latitudinal and longitudinal dependencies over West Africa compare to each other may be a topic for further studies.

Unlike vertical wind shear, our results suggest that thermodynamic conditions (measured by CAPE, CIN and 700 hPa DCAPE in this study) are of lesser importance for the horizontal growth of convective systems, but rather indicate the potential of their initial vertical development. In a similar fashion, Fink *et al.* (2006) found no substantial relationship between the magnitude of CAPE and CIN and the degree of convective organization which may be attributed to the lower dependence of cold-pool dynamics of higher organized systems on the thermodynamical condition to initiate new convective cells and thus to increase lifetime. However, CAPE, CIN and DCAPE tend to be highest for systems with intense deep convective cores (DCC and DWC, later combined to DEEP). Furthermore, as they are predominantly found early in the WAM season (March to May), the high values likely reflect the typical environmental conditions during this period, comparable to a regime described in Parker *et al.* (2005b) and also Vizy and Cook (2018). The poleward flank of the AEJ, where SWA is situated early in the year, is characterized by a moist low-level monsoon layer overlain by dry air of high potential temperature which may in some cases originate from the Sahara region through shallow dry convection (also Sultan and Janicot, 2003). Within the dry mid-levels, there is often a near-dry adiabatic lapse rate that can create a layer of high conditional instability and may favour the development of these deep convective cores once latent heat is released within the clouds. On the other hand, the mid-levels equatorward of the AEJ are more stable and moister and prevail particularly in the peak monsoon season in

July and August (termed the Sahelian phase in this study) over SWA, during which the occurrence of these deep core systems drops and that of non-organized, shallow warm-rain system is promoted. The relatively large differences of CAPE and DCAPE values between the deep core categories and shallow convection may reflect these contrasting mid-level regimes.

Low-level convergence and a subsequent increase of low-level moisture prior to the rainfall event is a common feature among all rainfall types. It is strongest in the case of mature MCSs whose convective and stratiform structures appear to be well captured by ERA-Interim. This specifically leads to a lowering of CIN (not shown) and higher PW, the latter being more a consequence of the system passage. This is consistent with the presumption of Dezfuli *et al.* (2017) that low-level convergence is a necessary condition for convection over West Africa. However, for the more humid SWA, the present study suggests that the absolute value of PW is not a suitable predictor for the different rainfall types, since the background PW is high. Similarly, Nicholls and Mohr (2010) showed that PW does not yield significant results for the prediction of the intensity of convective systems over West Africa, not even in the drier regions. The convergent motions and the associated increase of PW rather determine where convection in general is more likely to occur. That said, an investigation of the dynamic controls leading to moisture convergence was beyond the scope of this study and clearly warrants further and deeper analysis.

## 8.3 | Link between TRMM-PR and IR-based classification

Comparisons with IR-based classifications of convective systems of Lafore *et al.* (2017b) (C1–C4 classification) and Mathon *et al.* (2002) and Fink *et al.* (2006) (MCS-OCS classification) were performed by overlaying IR SEVIRI images onto the TRMM-PR snapshots. IR-based track information was used in the process to assign the TRMM-PR categories to classes defined by the above-referenced studies. This sequential approach was motivated by the fact that TRMM-PR does not provide continuous observations of rainfall and thus no information about the life-cycle of convective systems. Nesbitt and Anders (2009) have shown that the sampling error in a ten-year TRMM-PR rainfall climatology is still significant. Therefore, we investigated the relationship between TRMM-PR and IR-based rainfall systems with respect to lifetime and speed.

The degree of horizontal growth of a convective system is an indicator for the length of its lifetime. While mature MCSs (termed BSRs in this study) are almost exclusively long-lived systems (i.e. >9 h), less intense rainfall types are predominantly short-lived, diurnal phenomena. Furthermore, the majority of these BSRs (almost 70%) are fast-moving systems as well (i.e. a mean velocity of $\geq 10$ m s$^{-1}$). This is part of the definition of the C4 class in Lafore *et al.* (2017b) and of OCSs in Mathon *et al.* (2002) and Fink *et al.* (2006),

which is assumed to represent West African squall lines. Yet, the three MSCs-like systems are slower than in the Sahel, a finding consistent with Fink *et al.* (2006) and Lafore *et al.* (2017b), and tend to occur predominately during the early part of the first coastal rainy season. As the environment around BSR events show indications of AEWs, this can be considered as a testimony of the relevance of wave disturbances to the existence of squall lines (e.g. Fink and Reiner, 2003). However, not every AEW is accompanied by a BSR nor do BSRs solely develop under the presence of AEWs. It is further complicated by the fact that mid-level wave disturbances in SWA can be of non-AEW type (Knippertz *et al.*, 2017). Moreover, less intense rainfall systems, which typically occur in the absence of AEWs, can sometimes exhibit long lifetimes. This demonstrates that the understanding of the relationship between wave disturbances and rainfall systems can still be further improved.

## 9 | CONCLUDING REMARKS

Several other aspects of the paper require further exploration. Although pronounced differences in environmental conditions for the various rainfall types have been determined, this study has not investigated the conditions that lead to both their genesis and demise. One of the issues of using TRMM-PR data is the discontinuous observation of rainfall systems in space and time. The aforementioned combination with IR data and the subsequent exploitation of cloud tracking information is one way to gain a deeper understanding of the evolution of the rainfall types through their whole life-cycle as well as the (thermo-)dynamic conditions that control it. In this context, this paper has emphasized the relevance of (wave) disturbances for both enhancement and suppression of the organization of convective systems. Some cases of the interaction between mid-level vortices and rainfall systems were already highlighted in Knippertz *et al.* (2017) for June–July 2016. However, the implication of the occurrence of relevant disturbances for SWA, e.g. AEWs or Kelvin waves (Roundy and Frank, 2004), on the development of particular rainfall types needs to be studied in more detail. Additionally, this study focused on the influence of lower-tropospheric shear. In future work, it would be interesting to additionally investigate upper- or deep-level shear and its relation to the Tropical Easterly Jet.

In the light of interannual to decadal fluctuations of rainfall in SWA, further research is warranted to improve our knowledge of the relationship between disturbance and the type of rainfall from a dynamical but also a statistical point of view, ideally on a multi-year basis. First efforts were undertaken by Fink and Reiner (2003) on a two-year basis for AEWs over West Africa showing that a quarter of all AEWs were, in fact, not accompanied by an MSC. Finally, in the broader context of climate change, variables such as vertical wind shear may aid as a qualitative and statistical proxy for the assessment of the characteristics of rainfall and rainfall types in a future climate state over SWA.

## SUPPORTING INFORMATION

**File S1.** Supplementary material providing additional information on both the spatiotemporal variability of both rainfall categories and environmental conditions, which were discussed in sections 5 and 6, respectively.

Summary: In the present manuscript, the rainfall categories and environmental conditions were investigated representatively as composites for larger regions within southern West Africa (SWA). However, their spatiotemporal variability is high over SWA and has not been entirely addressed in the analysis. Thus, additional insight into this topic is given in the Supplementary material.

## REFERENCES

Acheampong, P.K. (1982) Rainfall anomaly along the coast of Ghana. Its nature and causes. *Geografiska Annaler, Series A: Physical Geography*, 64, 199–211.

Arkin, P.A. (1979) The relationship between fractional coverage of high cloud and rainfall accumulations during GATE over the B-scale array. *Monthly Weather Review*, 107, 1382–1387.

Aspliden, C.I., Tourre, Y. and Sabine, J.B. (1976) Some climatological aspects of West African disturbance lines during GATE. *Monthly Weather Review*, 104, 1029–1035.

Awaka, J., Iguchi, T., Kumagai, H. and Okamoto, K. (1997) Rain type classification algorithm for TRMM precipitation radar. In: *IEEE Geoscience and Remote Sensing Symposium, IGARSS'97. Remote Sensing – A Scientific Vision for Sustainable Development*, IEEE International, Singapore. Vol. 4, pp. 1633–1635

Bennartz, R. and Schroeder, M. (2012) Convective activity over Africa and the tropical Atlantic inferred from 20 years of geostationary Meteosat infrared observations. *Journal of Climate*, 25, 156–169.

Berrisford, P., Kållberg, P., Kobayashi, S., Dee, D.P., Uppala, S., Simmons, A., Poli, P. and Sato, H. (2011) Atmospheric conservation properties in ERA-Interim. *Quarterly Journal of the Royal Meteorological Society*, 137, 1381–1399.

Buckle, C. (1996) *Weather and Climate in Africa*. Longman, Harlow, UK.

Christensen, J.H., Krishna Kumar, K., Aldrian, E., An, S.-I., Cavalcanti, I.F.A., de Castro, M, Dong, W., Goswami, P., Hall, A., Kanyanga, J.K., Kitoh, A., Kossin, J., Lau, N.-C., Renwick, J., Stephenson, D.B., Xie, S.-P. and Zhou,

T. (2013) *Climate phenomena and their relevance for future regional climate change. Chapter 14*. Cambridge, UK: Cambridge University Press.

Dee, D.P., Uppala, S., Simmons, A., Berrisford, P., Poli, P., Kobayashi, S., Andrae, U., Balmaseda, M., Balsamo, G., Bauer, P., Bechtold, P., Beljaars, A.C.M., van de Berg, L., Bidlot, J., Bormann, N., Delsol, C., Dragani, R., Fuentes, M., Geer, A.J., Haimberger, L., Healy, S.B., Hersbach, H., Hólm, E.V., Isaksen, L., Kållberg, P., Kʹohler, M., Matricardi, M., McNally, A.P., Monge-Sanz, B.M., Morcrette, J.-J., Park, B.-K., Peubey, C., de Rosnay, P., Tavolato, C., Thépaut, J.-N. and Vitart, F. (2011) The ERA-Interim reanalysis: configuration and performance of the data assimilation system. *Quarterly Journal of the Royal Meteorological Society*, 137, 553–597.

Derrien, M. and Le Gléau, H. (2005) MSG/SEVIRI cloud mask and type from SAFNWC. *International Journal of Remote Sensing*, 26, 4707–4732.

Desbois, M., Kayiranga, T., Gnamien, B., Guessous, S. and Picon, L. (1988) Characterization of some elements of the Sahelian climate and their interannual variations for July 1983, 1984 and 1985 from the analysis of METEOSAT ISCCP data. *Journal of Climate*, 1, 867–904.

Dezfuli, A.K., Ichoku, C.M., Mohr, K. and Huffman, G.J. (2017) Precipitation characteristics in West and East Africa, from satellite and in-situ observations. *Journal of Hydrometeorology*, 18, 1799–1805.

Diatta, S. and Fink, A.H. (2014) Statistical relationship between remote climate indices and West African monsoon variability. *International Journal of Climatology*, 34, 3348–3367.

Duvel, J.P. (1989) Convection over tropical Africa and the Atlantic Ocean during northern summer. Part I: interannual and diurnal variations. *Monthly Weather Review*, 117, 2782–2799.

Duvel, J.P. (1990) Convection over tropical Africa and the Atlantic Ocean during northern summer. Part II: modulation by easterly waves. *Monthly Weather Review*, 118, 1855–1868.

Eldridge, R. (1957) A synoptic study of West African disturbance lines. *Quarterly Journal of the Royal Meteorological Society*, 83, 303–314.

Fink, A.H. and Reiner, A. (2003) Spatiotemporal variability of the relation between African easterly waves and West African squall lines in 1998 and 1999. *Journal of Geophysical Research: Atmospheres*, 108(D11). https://doi.org/10.1029/2002JD002816.

Fink, A.H., Vincent, D. and Ermert, V. (2006) Rainfall types in the West African Sudanian zone during the summer monsoon 2002. *Monthly Weather Review*, 134, 2143–2164.

Fink, A.H., Pohle, S. and Hoffmann, R. (2008) Spatial and temporal rainfall climatologies of Benin In *IMPETUS Atlas Benin: Research Results 2000–2007* pp. 21–22. Dept. of Geography, University of Bonn, Germany.

Fink, A.H., Engel, T., Ermert, V., van der Linden, R., Schneidewind, M., Redl, R., Afiesimama, E., Thiaw, W.M., Yorke, C., Evans, M. and Janicot, S. (2017) *Mean climate and seasonal cycle* pp. 1–39. Chichester, UK: John Wiley & Sons.

Fiolleau, T., Tomasini, M., Roca, R., Lafore, J., Laurent, H., Lebel, T. and Ramage, K. (2009) Summertime climatology of mesoscale convective systems over West Africa from 24 years of Meteosat observations. *Geophysical Research Abstracts*, 11. EGU General Assembly Conference, Vienna.

Fitzpatrick, R.G., Bain, C.L., Knippertz, P., Marsham, J.H. and Parker, D.J. (2015) The West African monsoon onset: a concise comparison of definitions. *Journal of Climate*, 28, 8673–8694.

Glickman, T.S. and Zenk, W. (2000) *Glossary of Meteorology*. American Meteorological Society, Boston, MA.

Guy, N., Rutledge, S.A. and Cifelli, R. (2011) Radar characteristics of continental, coastal, and maritime convection observed during AMMA/NAMMA. *Quarterly Journal of the Royal Meteorological Society*, 137, 1241–1256.

Hamilton, R.A., Archbold, J.W. and Douglas, C.K.M. (1945) Meteorology of Nigeria and adjacent territory. *Quarterly Journal of the Royal Meteorological Society*, 71, 231–264.

He, X., Kim, H., Kirstetter, P.E., Yoshimura, K., Chang, E.C., Ferguson, C.R., Erlingis, J.M., Hong, Y. and Oki, T. (2015) The diurnal cycle of precipitation in regional spectral model simulations over West Africa: sensitivities to resolution and cumulus schemes. *Weather and Forecasting*, 30, 424–445.

Heymsfield, G., Geerts, B. and Tian, L. (2000) TRMM precipitation radar reflectivity profiles as compared with high-resolution airborne and ground-based radar measurements. *Journal of Applied Meteorology*, 39, 2080–2102.

Houze, R.A., Jr (2004) Mesoscale convective systems. *Reviews of Geophysics*, 42, RG4003. https://doi.org/10.1029/2004RG000150.

Houze, R.A., Jr, Wilton, D.C. and Smull, B.F. (2007) Monsoon convection in the Himalayan region as seen by the TRMM Precipitation Radar. *Quarterly Journal of the Royal Meteorological Society*, 133, 1389–1411.

Houze, R.A., Jr, Rasmussen, K.L., Zuluaga, M.D. and Brodzik, S.R. (2015) The variable nature of convection in the tropics and subtropics: a legacy of 16 years of the Tropical Rainfall Measuring Mission satellite. *Reviews of Geophysics*, 53, 994–1021.

Huffman, G.J. and Norman, G.A., Jr (1988) The supercooled warm rain process and the specification of freezing precipitation. *Monthly Weather Review*, 116, 2172–2182.

Iguchi, T., Kozu, T., Meneghini, R., Awaka, J. and Okamoto, K. (2000) Rain-profiling algorithm for the TRMM precipitation radar. *Journal of Applied Meteorology*, 39, 2038–2052.

Janiga, M.A. and Thorncroft, C.D. (2014) Convection over tropical Africa and the east Atlantic during the West African monsoon: regional and diurnal variability. *Journal of Climate*, 27, 4159–4188.

Janiga, M.A. and Thorncroft, C.D. (2016) The influence of African easterly waves on convection over tropical Africa and the East Atlantic. *Monthly Weather Review*, 144, 171–192.

Judex, M. and Thamm, H.-P. (2008) *IMPETUS Atlas Benin – Research results 2000–2007*. Bonn, Germany: Department of Geography, University of Bonn.

Kamara, S.I. (1986) The origins and types of rainfall in West Africa. *Weather*, 41, 48–56.

Kawanishi, T., Kuroiwa, H., Kojima, M., Oikawa, K., Kozu, T., Kumagai, H., Okamoto, K., Okumura, M., Nakatsuka, H. and Nishikawa, K. (2000) TRMM precipitation radar. *Advances in Space Research*, 25, 969–972.

Kidd, C. (2001) Satellite rainfall climatology: a review. *International Journal of Climatology*, 21, 1041–1066.

Kidd, C. and Levizzani, V. (2011) Status of satellite precipitation retrievals. *Hydrology and Earth System Sciences*, 15, 1109–1116.

Knippertz, P., Fink, A.H., Deroubaix, A., Morris, E., Tocquer, F., Evans, M.J., Flamant, C, Gaetani, M., Lavaysse, C., Mari, C., Marsham, J.H., Meynadier, R., Affo-Dogo, A., Bahaga, T., Brosse, F., Deetz, K., Guebsi, R., Latifou, I., Maranan, M., Rosenberg, P.D. and Schlueter, A. (2017) A meteorological and chemical overview of the DACCIWA field campaign in West Africa in June–July 2016. *Atmospheric Chemistry and Physics*, 17, 10893–10918. https://doi.org/10.5194/acp-17-10893-2017.

Kummerow, C., Barnes, W., Kozu, T., Shiue, J. and Simpson, J. (1998) The tropical rainfall measuring mission (TRMM) sensor package. *Journal of Atmospheric and Oceanic Technology*, 15, 809–817.

Lafore, J.P., Chapelon, N., Beucher, F., Kane, M.D., Gaymard, A., Kasimou, A., Lepape, S., Mumbae, Z., Orji, B., Osika, D., Parker, D.J., Poan, E., Razafindrakoto, LG and Vincendon, J.C. (2017a) *West African synthetic analysis and forecast: WASA/F.* pp. 423–451. Chichester, UK: John Wiley & Sons.

Lafore, J.P., Chapelon, N., Diop, M., Gueye, B., Largeron, Y., Lepape, S., Ndiaye, O., Parker, D.J., Poan, E., Roca, R., Roehrig, R., Taylor, C. and Moncrieff, M. (2017b) *Deep convection* pp. 90–129. Chichester, UK: John Wiley & Sons.

Laing, A.G., Fritsch, J.M. and Negri, A.J. (1999) Contribution of mesoscale convective complexes to rainfall in Sahelian Africa: estimates from geostationary infrared and passive microwave data. *Journal of Applied Meteorology*, 38, 957–964.

Laing, A.G., Carbone, R., Levizzani, V. and Tuttle, J. (2008) The propagation and diurnal cycles of deep convection in northern tropical Africa. *Quarterly Journal of the Royal Meteorological Society*, 134, 93–109.

Le Barbé, L., Lebel, T. and Tapsoba, D. (2002) Rainfall variability in West Africa during the years 1950–90. *Journal of Climate*, 15, 187–202.

Levizzani, V., Schmetz, J., Lutz, H., Kerkmann, J., Alberoni, P. and Cervino, M. (2001) Precipitation estimations from geostationary orbit and prospects for METEOSAT Second Generation. *Meteorological Applications*, 8, 23–41.

Liu, C. (2011) Rainfall contributions from precipitation systems with different sizes, convective intensities, and durations over the tropics and subtropics. *Journal of Hydrometeorology*, 12, 394–412.

Liu, C. and Zipser, E.J. (2009) "Warm rain" in the tropics: seasonal and regional distributions based on nine years of TRMM data. *Journal of Climate*, 22, 767–779.

Mathon, V. and Laurent, H. (2001) Life cycle of Sahelian mesoscale convective cloud systems. *Quarterly Journal of the Royal Meteorological Society*, 127, 377–406.

Mathon, V., Laurent, H. and Lebel, T. (2002) Mesoscale convective system rainfall in the Sahel. *Journal of Applied Meteorology*, 41, 1081–1092.

Mohr, K.I. (2004) Interannual, monthly, and regional variability in the wet season diurnal cycle of precipitation in sub-Saharan Africa. *Journal of Climate*, 17, 2441–2453.

Molini, L., Parodi, A., Rebora, N. and Craig, G. (2011) Classifying severe rainfall events over Italy by hydrometeorological and dynamical criteria. *Quarterly Journal of the Royal Meteorological Society*, 137, 148–154.

Negri, A.J., Adler, R.F., Nelkin, E.J. and Huffman, G.J. (1994) Regional rainfall climatologies derived from Special Sensor Microwave Imager (SSM/I) data. *Bulletin of the American Meteorological Society*, 75, 1165–1182.

Nesbitt, S.W. and Anders, A.M. (2009) Very high resolution precipitation climatologies from the Tropical Rainfall Measuring Mission precipitation radar. *Geophysical Research Letters*, 36(15). https://doi.org/10.1029/2009GL038026.

Nicholls, S.D. and Mohr, K.I. (2010) An analysis of the environments of intense convective systems in West Africa in 2003. *Monthly Weather Review*, 138, 3721–3739.

Nicholson, S.E. (1979) Revised rainfall series for the West African subtropics. *Monthly Weather Review*, 107, 620–623.

Nicholson, S.E. (1981) Rainfall and atmospheric circulation during drought periods and wetter years in West Africa. *Monthly Weather Review*, 109, 2191–2208.

Nicholson, S.E. (2013) The West African Sahel: a review of recent studies on the rainfall regime and its interannual variability. *ISRN Meteorology*, 2013(453521). https://doi.org/10.1155/2013/453521.

Nolan, D.S., Zhang, C. and Chen, S. (2007) Dynamics of the shallow meridional circulation around intertropical convergence zones. *Journal of the Atmospheric Sciences*, 64, 2262–2285.

Omotosho, J.B. (1984) Spatial and seasonal variation of line squalls over West Africa. *Archives for Meteorology, Geophysics, and Bioclimatology, Series A*, 33, 143–150.

Omotosho, J. (1985) The separate contributions of line squalls, thunderstorms and the monsoon to the total rainfall in Nigeria. *International Journal of Climatology*, 5, 543–552.

Parker, D.J., Burton, R., Diongue-Niang, A., Ellis, R., Felton, M., Taylor, C., Thorncroft, C, Bessemoulin, P. and Tompkins, A. (2005a) The diurnal cycle of the West African monsoon circulation. *Quarterly Journal of the Royal Meteorological Society*, 131, 2839–2860.

Parker, D.J., Thorncroft, C.D., Burton, R.R. and Diongue-Niang, A. (2005b) Analysis of the African easterly jet, using aircraft observations from the JET2000 experiment. *Quarterly Journal of the Royal Meteorological Society*, 131, 1461–1482.

Parker, D.J., Kassimou, A., Orji, B.N., Osika, D.P., Hamza, I., Diop-Kane, M., Fink, A., Galvin, J.P.M., Guichard, F., Lamptey, B.L., Hamidou, H., van der Linden, R., Redl, R., Lebel, T. and Tubbs, C. (2017) Local weather. In *Meteorology of Tropical West Africa: The Forecasters Handbook* pp. 130–174. Parker, DJ, Diop-Kane, M (eds). John Wiley & Sons, Chichester, UK.

Reed, R.J., Norquist, D.C. and Recker, E.E. (1977) The structure and properties of African wave disturbances as observed during Phase III of GATE. *Monthly Weather Review*, 105, 317–333.

Riemann-Campe, K., Fraedrich, K. and Lunkeit, F. (2009) Global climatology of convective available potential energy (CAPE) and convective inhibition (CIN) in ERA-40 reanalysis. *Atmospheric Research*, 93, 534–545.

Roca, R., Aublanc, J., Chambon, P., Fiolleau, T. and Viltard, N. (2014) Robust observational quantification of the contribution of mesoscale convective systems to rainfall in the tropics. *Journal of Climate*, 27, 4952–4958.

Romatschke, U. and Houze, R.A. (2010) Extreme summer convection in South America. *Journal of Climate*, 23, 3761–3791.

Romatschke, U., Medina, S. and Houze, R.A. (2010) Regional, seasonal, and diurnal variations of extreme convection in the South Asian region. *Journal of Climate*, 23, 419–439.

Rotunno, R., Klemp, J.B. and Weisman, M.L. (1988) A theory for strong, long-lived squall lines. *Journal of the Atmospheric Sciences*, 45, 463–485.

Roundy, P.E. and Frank, W.M. (2004) A climatology of waves in the equatorial region. *Journal of the Atmospheric Sciences*, 61, 2105–2132.

Rowell, D.P. and Milford, J.R. (1993) On the generation of African squall lines. *Journal of Climate*, 6, 1181–1193.

Schrage, J.M., Fink, A.H., Ermert, V. and Ahlonsou, E.D. (2006) Three MCS cases occurring in different synoptic environments in the sub-Sahelian wet zone during the 2002 West African monsoon. *Journal of the atmospheric sciences*, 63, 2369–2382.

Schröder, M., König, M. and Schmetz, J. (2009) Deep convection observed by the Spinning Enhanced Visible and Infrared Imager on board Meteosat 8: spatial distribution and temporal evolution over Africa in summer and winter 2006. *Journal of Geophysical Research: Atmospheres*, 114(D5). https://doi.org/10.1029/2008JD010653.

Schumacher, C. and Houze, R.A. (2003) The TRMM precipitation radar's view of shallow, isolated rain. *Journal of Applied Meteorology*, 42, 1519–1524.

Sultan, B. and Janicot, S. (2003) The West African monsoon dynamics. Part II: The "preonset" and "onset" of the summer monsoon. *Journal of Climate*, 16, 3407–3427.

Taylor, C.M., Belušić, D., Guichard, F., Parker, D.J., Vischel, T., Bock, O., Harris, P.P., Janicot, S., Klein, C. and Panthou, G. (2017) Frequency of extreme Sahelian storms tripled since 1982 in satellite observations. *Nature*, 544(7651), 475–478.

Thiao, W., Cadet, D. and Desbois, M. (1990) A note on: estimation of rainfall due to squall lines over West Africa using METEOSAT imagery. *Meteorology and Atmospheric Physics*, 42, 69–76.

Thorncroft, C.D., Nguyen, H., Zhang, C. and Peyrille, P. (2011) Annual cycle of the West African monsoon: regional circulations and associated water vapour transport. *Quarterly Journal of the Royal Meteorological Society*, 137, 129–147.

Tjemkes, S.A. (2005) *On the conversion from radiances to equivalent brightness temperatures*. Available at: http://www.eumetsat.int/groups/ops/documents/document/pdf_msg_seviri_rad2bright.pdf. [Accessed: 4 December 2017]

Vizy, E.K. and Cook, K.H. (2018) Mesoscale convective systems and nocturnal rainfall over the West African Sahel: role of the Inter-tropical front. *Climate Dynamics*, 50, 587–614.

Vogel, P., Knippertz, P., Fink, A.H., Schlueter, A. and Gneiting, T. (2018) Skill of global raw and postprocessed ensemble predictions of rainfall over northern tropical Africa. *Weather and Forecasting*, 33(2), 369–388. https://doi.org/10.1175/WAF-D-17-0127.1.

Vollmert, P., Fink, A.H. and Besler, H. (2003) 'Ghana Dry Zone' und 'Dahomey Gap': Ursachen für eine Niederschlagsanomalie im tropischen Westafrika. *Erde*, 134(4), 375–393.

Williams, M. and Houze, R.A., Jr (1987) Satellite-observed characteristics of winter monsoon cloud clusters. *Monthly Weather Review*, 115, 505–519.

Yang, G.Y. and Slingo, J. (2001) The diurnal cycle in the tropics. *Monthly Weather Review*, 129, 784–801.

Young, M.P., Chiu, J.C., Williams, C.J.R., Stein, T.H.M., Stengel, M., Fielding, M.D. and Black, E. (2018) Spatio-temporal variability of warm rain events over southern West Africa from geostationary satellite observations for climate monitoring and model evaluation. *Quarterly Journal of the Royal Meteorological Society*. https://doi.org/10.1002/qj.3372.

Zhang, C., Nolan, D.S., Thorncroft, C.D. and Nguyen, H. (2008) Shallow meridional circulations in the tropical atmosphere. *Journal of Climate*, 21, 3453–3470.

Zuluaga, M.D. and Houze, R.A. (2013) Evolution of the population of precipitating convective systems over the equatorial Indian Ocean in active phases of the Madden–Julian oscillation. *Journal of the Atmospheric Sciences*, 70, 2713–2725.

Zuluaga, M.D. and Houze, R.A. (2015) Extreme convection of the near-equatorial Americas, Africa, and adjoining oceans as seen by TRMM. *Monthly Weather Review*, 143, 298–316.